1-1-2011

# Synthesis Of Nanoparticle Networks By Femtosecond Laser Ablation Of Microparticles

Paineet S. Waraich
*Ryerson University*

# SYNTHESIS OF NANOPARTICLE NETWORKS BY FEMTOSECOND LASER ABLATION OF MICROPARTICLES

by

Palneet Singh Waraich
Bachelor of Engineering
Ryerson University, 2009

A Thesis
presented to Ryerson University

in partial fulfillment of the
requirements for the degree of
Master of Applied Science
in the Program of
Mechanical Engineering

Toronto, Ontario, Canada, 2011

# AUTHOR'S DECLARATION

I hereby declare that I am the sole author of this thesis.

I authorize Ryerson University to lend this thesis to other institutions or individuals for the purpose of scholarly research.

**Palneet Singh Waraich**

**Ryerson University**

I further authorize Ryerson University to reproduce this thesis by photocopying or by other means, in total or in part, at the request of other institution or individuals for the purpose of scholarly research.

**Palneet Singh Waraich**

**Ryerson University**

# ABSTRACT


## SYNTHESIS OF NANOPARTICLE NETWORKS BY FEMTOSECOND LASER ABLATION OF MICROPARTICLES

Palneet Singh Waraich, Master of Applied Science, 2011

Department of Mechanical and Industrial Engineering, Ryerson University

The process of laser ablation has been adapted to generate nanoparticles from microparticles of the material, referred to as laser ablation of microparticles (LAM). The LAM process has been shown to generate finer nanoparticles than were previously possible through laser ablation of solid targets.

In this thesis, a method of generating a 3D nanoparticle network using the LAM process has been proposed using a femtosecond laser. 3D nanoparticles were successfully generated through ablation of microparticle samples of lead oxide, nickel oxide and zinc oxide. The size of the nanoparticles in the generated network was significantly reduced in comparison with similar networks generated through laser ablation of solid targets. The method has been further extended to generate a unique alloy nanomaterial through the ablation of the microparticle containing powders of two metals (Aluminum and Nickel Oxide).

# ACKNOWLEDGEMENTS

I take this opportunity to pay my deep sense of gratitude and sincere thanks to my research supervisors Dr. K. Venkatakrishnan and Dr. Bo Tan for their constant interest, encouragement and invaluable guidance throughout the present work and rendering facilities for the completion of this research study.

I would like to thank all the faculty members, technical officers and administrative staff members for their kind support and cooperation all the time during my stay at Ryerson University.

I am also grateful to my family and friends for their continued support, prayers and love.

# DEDICATION

The author hereby would like to dedicate this thesis to his parents as a token of appreciation for their invaluable love and support.

# TABLE OF CONTENTS

# LIST OF FIGURES

# LIST OF APPENDICES

# NOMENCLATURE

| | |
|---|---|
| ns | Nanosecond ($10^{-9}$ s) |
| ps | Picosecond ($10^{-12}$ s) |
| fs | Femtosecond ($10^{-15}$ s) |
| μs | Microsecond ($10^{-6}$ s) |
| ms | Millisecond ($10^{-3}$ s) |
| nm | Nanometer ($10^{-9}$ m) |
| μm | Micrometer ($10^{-6}$ m) |
| cm | Centimeter ($10^{-3}$ m) |
| in | Inches |
| MHz | Megahertz ($10^{6}$ Hz) |
| kHz | Kilohertz ($10^{3}$ Hz) |
| W | Watt (J/s) |
| GW | Gigawatt ($10^{9}$ J/s) |
| eV | Electron Volt |
| K | Kelvin |
| $^{o}$C | Degree Celsius |
| J | Joule |
| μJ | Micro-Joule ($10^{-6}$ J) |
| 2D | 2 Dimensional |
| 3D | 3 Dimensional |
| UV | Ultra violet |

| | |
|---|---|
| $T_e$ | Electron temperature |
| $T_i$ | Lattice temperature |
| I(t) | Laser intensity at time t |
| $\alpha$ | Absorption coefficient |
| $k_e$ | Electron thermal conductivity |
| $I_0$ | Intensity |
| t | Time |
| $\tau_L$ | Laser pulsewidth |
| $\tau_e$ | Electron cooling time |
| $\tau_i$ | Lattice heating time |
| $F_a$ | Ablation fluence |
| $F_{th}$, $ø_{th}$ | Threshold fluence |
| D | Heat diffusion coefficient |
| $\rho$ | Density |
| P | Average power of the laser pulse |
| R | Reflection coefficient |
| r | Reciprocal of pulse interval |
| $I_{th}$ | Threshold intensity |
| F | Laser fluence |
| $T_0$ | Temperature at time t = 0 |
| $T_i$ | Initial temperature |
| $\omega_0$ | Radius of the laser focal spot |
| $\lambda_0$ | Wavelength of the laser beam |

# Chapter 1: Introduction

## 1.1 Nanoparticles and Their Applications

The term nanoparticle refers to particles which have a diameter of 100nm or less. They have also been termed as ultra-fine particles. Nanoparticles have attracted a great deal of attention from the scientific community because of their enhanced optical, chemical and electrical properties in comparison to their macro counterparts. These enhanced properties are mainly due to large surface-to-volume ratio and the effect of quantum confinement. The advanced properties of the nanoparticles make them highly desirable for use in the development of different technological applications through advances in nanoscience and nanotechnology.

The small size of the nanoparticles is responsible for the difference in properties in comparison to bulk materials. Some examples of the different properties of the nanoparticles are lower melting temperature [1], increased solid-solid phase transition pressure [2], decreases ferroelectric phase transition temperature [3], higher self-diffusion coefficient [4], modified thermophysical properties [5] and enhanced catalytic activity [6].

The superior properties of the nanoparticles compared to their bulk materials makes them highly desirable for use in enhancing the existing technologies and developing emerging technologies for the 21$^{st}$ century. Some of the applications of nanoparticles have been described below.

### 1.1.1 Nanoparticles as quantum dots

Nanoparticle as a system can be referred to as a quantum dot or a zero dimension (0-D) structure. For such a system, the confinement of the electrons in a small domain results in new energy levels that are determined by quantum confinement effects. The creation of these new energy levels gives nanoparticles modified optoelectronic properties in comparison to the bulk material. These optoelectronic property modifications can be utilized for the development and enhancement of several electronic and optical devices. One of the fields where such properties have been used is the field of light emitting diodes (LEDs). Nanoparticles of CdSe have been used in voltage controlled LEDs, where red or green color is emitted based on the voltage applied [7]. Quantum dots can also be used in memory storage devices, where they can be arranged in a 3D array to which information can be written to and retrieved from. They can also be utilized to reduce the response time of a lot of microelectronic devices thus increasing their working efficiency [8].

### 1.1.2 Biomedical Applications

The small size of the nanoparticles which is similar to that of biomolecules such as proteins makes them an excellent choice for biomedical applications. Nanoparticles can be used for applications such as drug delivery, bioimaging and biosensing etc. For diagnosis and other biomedical applications, the sensing of biological agents is very important. The unique physicochemical properties of the nanoparticles make them a suitable candidate for sensing applications. Some of the types of sensing techniques where nanoparticles have been successfully used are colorimetric sensing, fluorescence sensing and electrochemical sensing. The efficacy of the drugs can be enhanced by the use of drug delivery systems (DDS) which

improve the solubility and the bio-distribution of the drugs. The ability of the nanoparticles to conjugate with biomolecules such as proteins and DNA make them a potential DDS. [9]

### 1.1.3 Gas Sensors

A gas sensor consists of a material with measurable physical properties (electrical or chemical) which change in the presence of a gas. A number of nanoparticle baser gas sensor systems have been developed. Palladium nanoparticles, in the size range of 10-15nm, were used for the detection of hydrogen gas in a Pd-H system based gas sensor [10]. The use of nanoparticles in gas sensors has been shown to increase the sensitivity and improved the gas selectivity in comparison to non-nanoparticle based sensors [11].

## 1.2 Nanoparticle Synthesis: Traditional Methods

Over the years, many methods have been used for the synthesis of nanoparticles. New methods are being researched and developed for the efficient generation of nanoparticles from a vast variety of materials. The generation of nanoparticles can be divided into two distinct approaches; top-down approach and bottom-up approach. The schematic in Figure 1-1 shows an illustration for the generation of the nanoparticles from the two approaches. In this section we discuss some of the methods for nanoparticle generation.

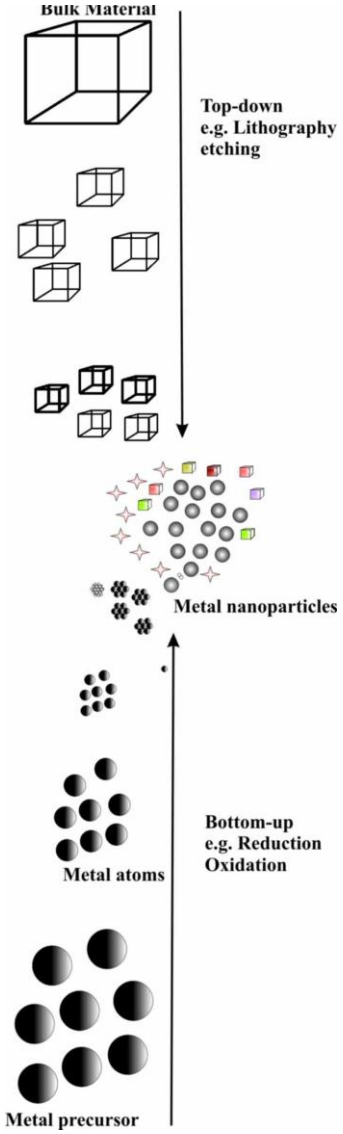


Figure 1-1: Illustrative representation of top-down and bottom-up approaches for generation of nanoparticles [12]

### 1.2.1 Inert Gas Condensation

It is one of earliest used methods for the synthesis of nanoparticles. It is well suited for the generation of nanoparticles from metals. Under this method, a solid material is heated till its evaporation point. The vapors are then mixed with a cool inert gas which rapidly cools them to form nanoparticles. Nanocomposites or other compounds can also be achieved by inserting a

reactive gas in the environment. Extensive research has been carried out to better control the size of the generated nanoparticles. It has been shown that the flow and mixing of the cool gas and the hot vapors as well as the pressure and the molecular weight of the inert gas affects the size of the nanoparticles generated. This method has been used for generating nanoparticles in the size range of 5nm to a few hundred nm. [8]

### 1.2.2 Sputtering

Sputtering is the method of vaporizing material from the surface of a solid through bombardment of high-velocity ions of an inert gas (or electrons) in vacuum, causing an ejection of atoms or clusters. As early as in 1982, nanoparticles of Ti and Al with size as small as 10nm were produced by this method [13]. One of the advantages of this method is that the incident ion or electron beam only heats the target material and thus the generated nanoparticles comprises mainly of the target material.

### 1.2.3 Laser Vaporization

This technique uses a laser which evaporates a sample target in an inert gas flow reactor. The source material is locally heated to a high temperature enabling vaporization. The vapor is cooled by collisions with the inert gas molecules and the resulting supersaturation induces nanoparticle formation. This method has been used for generating nanoparticles in the size range of 6 – 100nm from powders, single crystals and sintered blocks [14]. A modified method which combines laser vaporization of metal targets with controlled condensation in a diffusion cloud chamber was used to synthesize nanoscale metal oxide and metal carbide particles with a size range of 10-20 nm [15].

### 1.2.4 Mechanical Attrition

Mechanical attrition is a 'top-down' method of generating nanoparticles. In this process, nanoparticles are formed in a mechanical device in which energy is imparted to a course grained material to reduce particle size. The final size of the particles obtained depends on the milling time that the material has been exposed to. At long enough milling times, nanoparticles with sizes of 10 – 15nm has been obtained [16]. Figure 1-2 gives an example of the nanoparticles generated by this method.

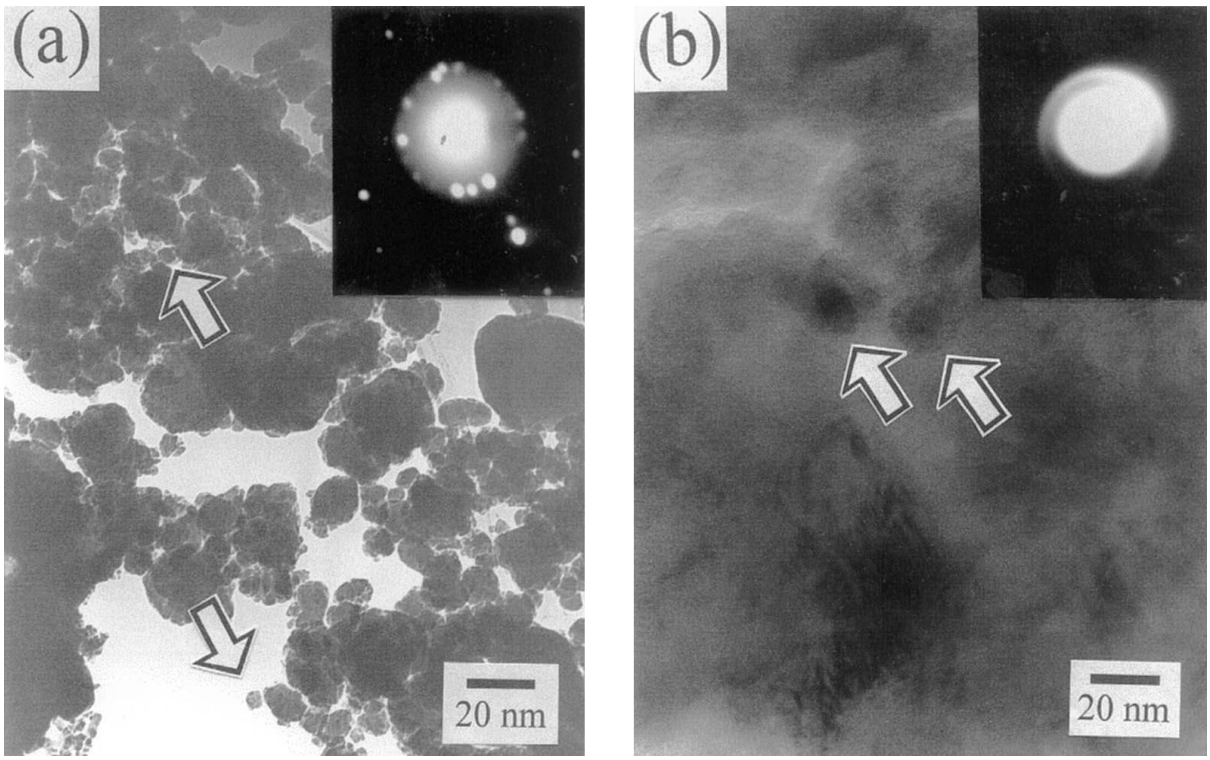


Figure 1-2: Nanoparticles obtained at different milling times a) 240hours; b) 168hours [16]

## 1.3 Nanoparticle Synthesis: Laser Ablation Methods

The development of powerful lasers has opened up many new areas where laser processing can be used. One of the areas where laser processing has rapidly grown is the field of nanotechnology; specifically the development of laser ablation based methods for nanoparticle synthesis. The laser ablation methods for nanoparticle synthesis have been reviewed in this section.

### 1.3.1 Laser Ablation

Laser ablation is a technique where laser pulses are used to ablate a solid target placed in a gaseous or liquid environment leading to nanoparticle formation in form of nanopowder or colloidal solution. It is a straight forward method of generating nanoparticles in comparison to other traditional methods. Some of the advantages of the laser ablation method are;

- Does not require long reaction times, high temperature environment.
- Is free of multi-step chemical synthesis.
- Can produce nanoparticles from vast range of materials ranging from metals to polymers to dielectric materials
- The use of toxic and hazardous chemical precursors is not required
- Nanoparticles produced in a vacuum or liquid are free of contaminants and thus can be used for biomedical applications

The first ever generation of nanoparticles by the use of laser ablation was reported in 1981, where a Q-switched Nd:YAG laser was used for the generation of Cu clusters, then characterised as ultrafine particles [17]. In this method, laser ablation was combined with supersonic

expansion into vacuum. The method of laser ablation has since been greatly researched and refined for the generation of nanoparticles from a vast range of materials.

M. Fumitaka et. al. (2000) produced nanoparticles of silver through laser ablation of a silver plate in aqueous solution of surfactants. The silver metal plate was placed in an aqueous solution of the surfactant $C_nH_{2n+1}SO_4Na$; different surfactants were used with n=8, 10, 12 and 14. The ablation was carried out with a Nd:YAG laser having a pulse width of 10ns. Nanoparticles with an average size of ~10nm were reported to have been produced [18]. Figure 1-3a gives an example of the nanoparticles generated through this method.

In another work, nanoparticles of gold were produced by ablation of a gold plate in an SDS solution using a Nd:YAG laser with a pulse width of 10ns. The variation in the size of the nanoparticles with varying concentrations of the SDS was studied. It was observed that the size of the gold nanoparticles decreased with an increase in the concentration of SDS [19]. Figure 1-3b gives an example of the nanoparticles generated through this method. The use of SDS or other surfactants during laser ablation of a target in a liquid environment results in a reduced size distribution of the nanoparticles [18-20]. However Kabashin and Meunier reported nanoparticles in the size range of 3nm – 10nm by ablation of a gold target in pure deionized water [21].

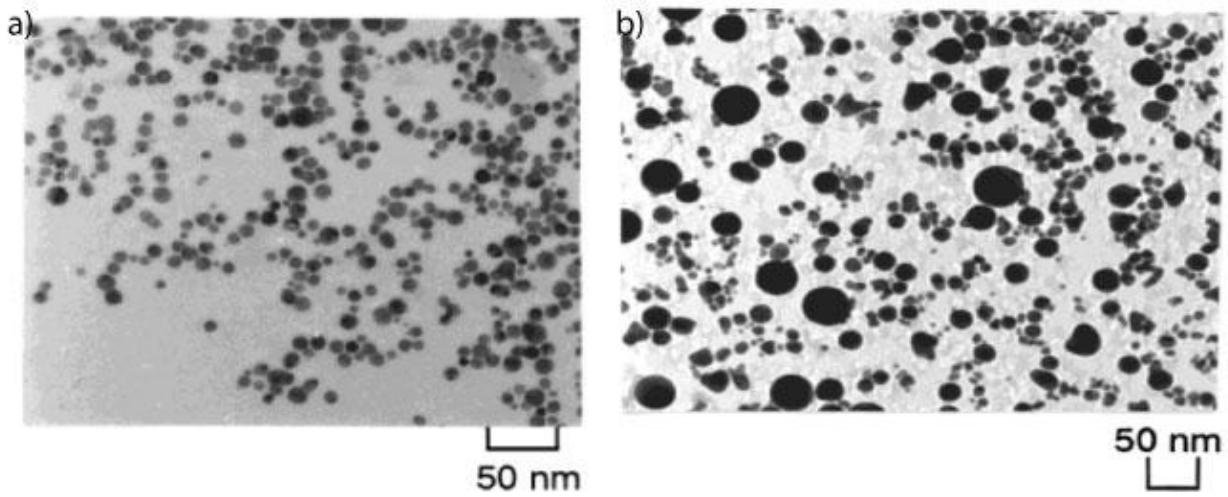


Figure 1-3: Nanoparticles produced by laser ablation of: a) Silver [18]; b) Gold [19] in an aqueous solution of SDS

The work reviewed above focused on the dependence of nanoparticle size distribution on the characteristics of the environment in which the target was placed. Another parameter of laser ablation that has been examined is the wavelength of the laser beam and its effect on the size of the generated nanoparticles. Tsuji et. al. have studied the effect of laser wavelength on particle size. In their work, a silver metal target placed in a liquid environment of deionized water was ablated at wavelengths of 1064nm, 532nm and 355nm at a laser fluence of 36J/cm$^2$. It was observed that the size of the nanoparticles went from 29nm to 12nm with the decrease in the wavelength of the laser beam. Thus the wavelength of the laser beam was shown to have an effect on the size of the nanoparticles generated [22].

The generation of nanoparticles through laser ablation has been restricted only to the ablation of target in a liquid environment. Research has also been done on the generation of nanoparticles by laser ablation in vacuum and in a background gas environment (air or other gases). In one such study, a Ti:sapphire laser with a pulse width of 120fs was used in the ablation of silicon target in

vacuum. The nanoparticles had a size distribution with a radius between 5nm and 25nm [23]. Figure 1-4 gives an example of the nanoparticles generated through this method. The analysis of the results indicated that nanoparticle formation did not occur through condensation process in a dilute atomic vapour, rather the nanoparticles were formed near the target surface as a result of ultrashort non-thermal melting and the consequent expansion into the vacuum of the material through extremely high temperatures and pressure created by the intense femtosecond laser pulse [23, 24].

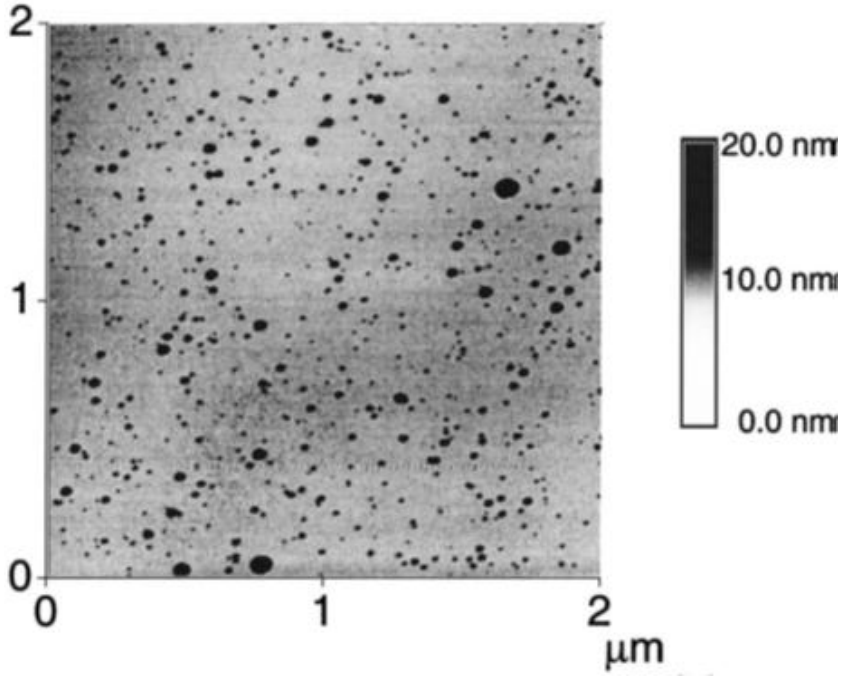


Figure 1-4: Silicon nanoparticles produced by femtosecond laser ablation of Si target in vacuum [23]

The above section provided a review of the work that has been done in the field of nanoparticle generation through laser ablation. The mechanism for the generation of nanoparticles by laser ablation will be discussed in Chapter 2.

### 1.3.2 Laser Ablation of Microparticles (LAM)

A new method of laser ablation has been studied in which the target material is not solid but is comprised of microparticles of the material of which nanoparticles are to be produced. This method is known as laser ablation of microparticles (LAM). The method of LAM capitalizes on the lack of a strong bonding between the microparticles to generate much finer nanoparticles at much lower laser energy than required for a solid feedstock target.

The LAM process has been used for the generation of nanoparticles from glass microspheres [25], metal microparticles [26, 27] and alloys [26]. In the reported literature the microparticles were either applied on a substrate or were in a flowing aerosol when exposed to the laser. The generated nanoparticles were collected on a collector plate placed a certain distance away from the target surface. In all the cases, the nanoparticles were collected in a non-agglomerated state. A significant reduction in the size of the generated nanoparticles was observed when compared to the size of the nanoparticles generated through ablation of solid targets.

C. Juang et. al. used an excimer laser with a wavelength of 249nm and a pulse width of 12ns to irradiate micron sized particles under normal atmospheric conditions. Soda lime glass microspheres with a mean diameter of 8μm were used for the experiment. An analysis was carried out on the size and the size distribution of the generated particles and their dependence on laser fluence. The experiments were carried out at laser fluence of 4.5, 6.0 and 7.5 J/cm$^2$. The particles generated for each fluence setting were collected on a silicon substrate and analysed under a Scanning Electron Microscope (SEM). It was observed that the generated nanoparticles ranged in size from 20nm to 190nm for all the three cases. It was also noted that for the lowest

fluence, a peak in particle size distribution was observed at 80nm which shifted to 60nm for the highest fluence [25]. Figure 1-5 gives an example of the nanoparticles generated through this method.

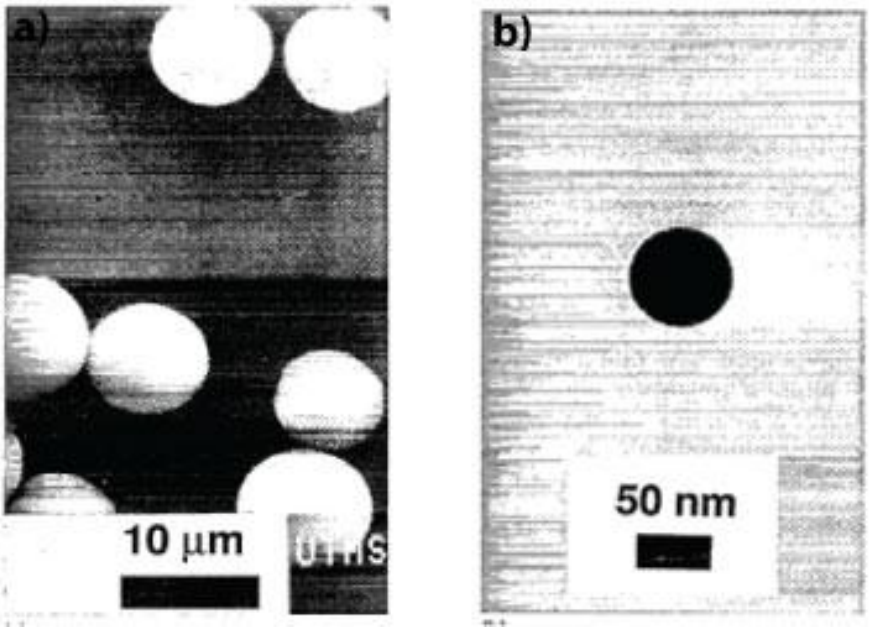


Figure 1-5: Laser ablation of glass microspheres; a) starting microspheres, b) generated glass nanoparticle [25]

In another work, M.F. Becker et. al. used the process of LAM to ablate feedstock (comprised of micron sized powder) of silver, gold and permalloy to form nanoparticles. An excimer laser with a pulse width of 12ns was used to ablate the feedstock microparticles applied on to the surface of a UV transparent quartz slide. The microparticles had an average size of 2µm to 4µm and were dispersed on the quartz slide from a methanol suspension. The sample was ablated at different laser fluence. An increase in the mean diameter of the generated nanoparticles was observed with the increase in the laser fluence (opposite to the observation for glass microspheres, where the

diameter decreased with increasing laser fluence). The generated nanoparticles shown in Figure 1-6 had a mean diameter in the range of 10nm to 100 nm.

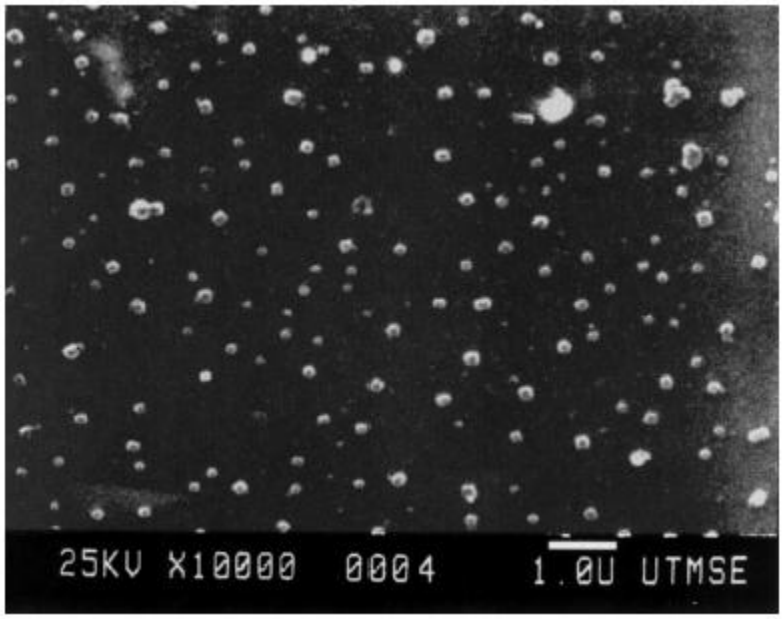


Figure 1-6: SEM image of the nanoparticles generated by laser ablation of gold microspheres [27]

Apart from the generation of nanoparticles by the ablation of microparticles applied on a substrate, the LAM process was also used for generating nanoparticles from a flowing aerosol containing microparticles. In their work, W.T. Nichols et. al. reported the production of nanoparticles through laser ablation of a flowing aerosol of microparticles of silver. Silver microparticles with a mean size of 1.5μm in a flowing aerosol of nitrogen gas were ablated by an excimer laser at fluence ranging from 0.3J/cm$^2$ to 4.2J/cm$^2$. The generated nanoparticles were collected on an electrostatically charged carbon grid and analysed for size distribution. For all the cases, the nanoparticles obtained were spherical, non-agglomerated and were less than 20nm in size. [28]

The breakdown of the microparticles into nanoparticles has been explained on the basis of plasma breakdown and shockwave propagation through the microparticles. As per this theory, as the breakdown threshold of the material is achieved, a shockwave is generated. The shockwave propagates in two different directions; the primary shockwave propagates away from the material while the secondary shockwave propagates towards the material. As the shockwave travels through the feedstock, it compresses and heats the material to above its critical point. When the shockwave passes, the region right behind it has a much lower pressure which causes rapid condensation of the material. This rapid condensation leads to the formation of nanoparticles.

The major advantage of the LAM process is the reduction in the amount of laser energy required to completely vaporize the metal particle; for the gold particles it was observed that total laser energy absorbed for complete vaporization was 25% of the net energy required. Due to the loosely packed nature of the microparticles, less laser energy is required for the initiation of the ablation process than compared to a solid target.

## 1.4 Research Objectives

The LAM process has been successfully used for the generation of nanoparticles from microparticles. This research will focus on microparticle ablation using a Mega-Hertz repetition rate femtosecond laser, with the aim of producing nanostructure of reduced particle size. In particular, the following studies will be conducted:

- Investigate mega-hertz repetition rate femtosecond laser ablation of microparticles. The nanostructure generated will be compared to similar structures generated through laser ablation of solid targets (Metals: Lead, Gold; Semi-conductor: Silicon; Dielectric: Glass)
- LAM method for the generation of nanostructure will be examined for its use in the generation of an alloy nanostructure from pre-mixed two independent microparticle powders.
- This study will also probe the feasibility of the LAM process in generating a nanostructure by the interaction of two materials, one in solid phase and the other in powder phase.

## 1.5 Thesis Outline

Chapter 2 of the thesis will be focused on the explanation of the process of laser ablation of solids. It will also give a detailed insight into the generation of nanoparticles through laser ablation. The last section of the chapter will be focused on the process of laser ablation of microparticles (LAM).

Chapter 3 describes the experimental set-up that was used during the course of the study. The methods of sample preparation of the experiments are also mentioned in this chapter

Chapter 4 gives an in-depth look into the generation of a 3D nanostructure through laser ablation of metallic microparticles. Experimental parameters and results are mentioned in this chapter. A section of the chapter is devoted to explaining the proposed mechanism for the nanostructure generation

Chapter 5 discusses the results of the experiment performed on the mixture of Al and NiO microparticles to obtain a combined nanostructure. A proposed mechanism for the mixing of the nanoparticle of the two microparticle powders through the ablation process is also talked about in this chapter. The results of the ablation of a microparticle powder on an aluminum foil are also presented.

Chapter 6 concludes the thesis and talks about the future work that can be done in this field of research.

# Chapter 2: Laser Ablation for Nanoparticle Synthesis

## 2.1 Laser ablation process

Before the generation of nanoparticles through laser ablation can be discussed, a better understanding of laser ablation as a process is required. This section provides an in-depth analysis into the process of laser ablation; fundamentals of the process and the proposed mechanisms are discussed in detail.

Laser ablation refers to the process of material removal from the surface of the material upon irradiation by a laser beam. This technique has been in existence since the invention of the laser, where initially it was used for thin-film deposition. Only recently, has the laser ablation process been used in material processing other than pulsed laser deposition (PLD) and UV lithography etc. Laser ablation is based on the principle of capitalising on the high power laser pulses for the evaporation of a small amount of matter from the surface of the target.

As the laser pulse hits the target, photons are absorbed in the surface layer via electronic processes. The absorbed energy gets transferred into the material by either electrons (in case of metals) or phonons (in case of non-metals). The relaxation time for metals ($\sim 10^{-14}$s) is much faster than for non-metals ($> 10^{-12}$s), though when compared with the laser pulse duration the absorbed energy gets rapidly converted into heat. The absorbed energy heats the surface to beyond the melting point of the material. The melted surface begins to vaporize and the very high temperatures present at the surface cause ejection of molecules of the target.

In addition to the interaction between the laser and the target, laser-plasma, plasma-target, laser-vapour and vapour-target interaction play an important role in the laser ablation process. One of the most important laser parameters for ablation is the laser pulse energy density (laser fluence) on the target surface. For sufficiently high laser fluence, rapid evaporation of the material occurs from a thin surface layer. This points to the existence of laser ablation threshold i.e for every material there exists a minimum laser fluence value (threshold fluence) below which ablation does not occur. The ablation rate increases non-linearly with increase in laser power density above the ablation threshold.

The laser ablation process can be broken into three different steps: energy absorption, energy transfer and breakdown. The initiating step in laser ablation is the absorption of the laser energy by the target material, accomplished by either linear or nonlinear processes. The material in the focal region is heated to melting temperature and, depending on laser intensity and pulsewidth, subsequently to vaporization temperature. The absorption mechanisms depend on laser intensity, hence on laser pulse-widths for a given laser fluence. For metals and semiconductors, the main absorption mechanism for longer pulse-widths in linear absorption while nonlinear absorption becomes dominant at ultrashort pulse-widths. For dielectric materials, absorption has to come from nonlinear processes through laser-induced optical breakdown. Laser-induced breakdown is a process where a normally dielectric material is first transformed into absorbing plasma by the strong laser pulse. Subsequent absorption by the plasma of the laser energy causes heating that leads to irreversible damage to the host material. The nonlinear processes that cause breakdown are avalanche ionization and multiphoton ionization.

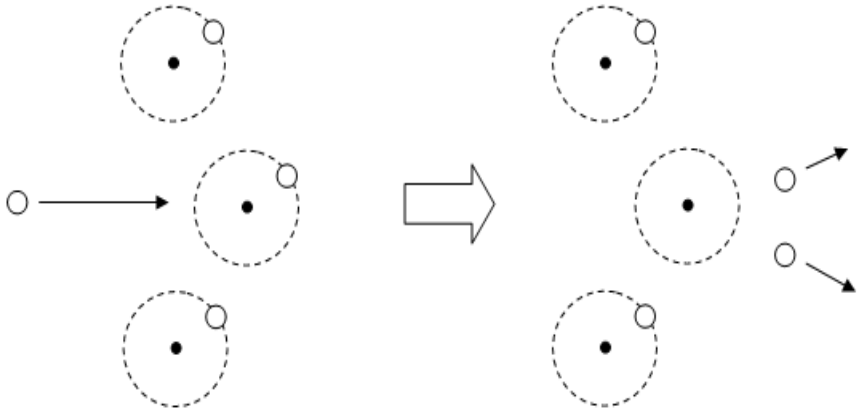

Figure 2-1: Illustration of avalanche ionization [29]

In a dielectric material, the bound valence electrons have an ionization potential or bandgap greater than the laser photon energy. The bound electrons do not absorb the laser light at low intensities. However, in any material there are always some free or conduction electrons present, and they are the seed electrons for avalanche ionization as illustrated in Figure 2-1. The free electron can absorb laser energy when it collides with the bound electrons and the lattice through dephasing. This is the Joule heating process, also known as inverse Bremsstrahlung. The seed electron can be accelerated enough that its kinetic energy exceeds the ionization potential of the bound electron. Therefore the next collision with a bound electron will result in an ionization event if the free electron transfers nearly all its energy to the bound electron, resulting in two free electrons with low kinetic energies. This is called impact ionization. This process will repeat itself, leading to an avalanche where the free-electron density grows exponentially from the very low seed electron density. When enough bound electrons are ionized by this avalanche process, plasma with a critical density is created, and the dielectric material is broken down and becomes absorbing.

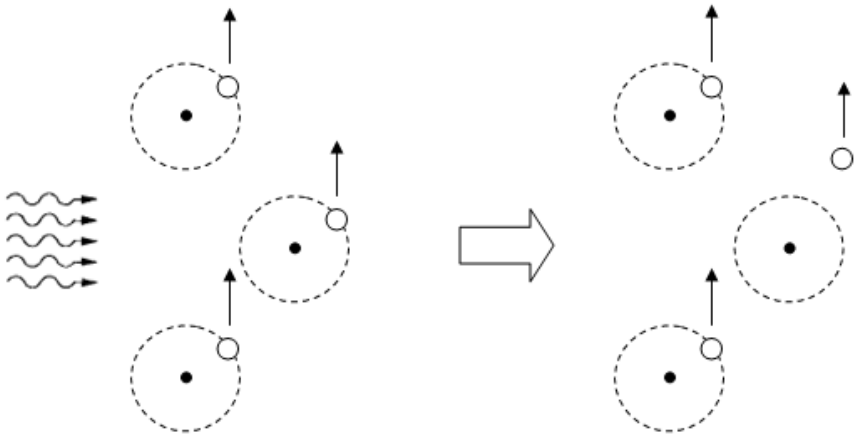

Figure 2-2: Schematic for multiphoton ionization [29]

In case of ultrashort laser pulse – matter interaction, the laser field strength is very high for bound electrons of the dielectric material to be directly ionized through multiphoton absorption as illustrated in Figure 2-2. A bound electron can be lifted from its bound energy level or valence band to the free energy level or conduction band by simultaneously absorbing ‘m’ photons in the laser pulse. This is called multiphoton ionization. The laser-induced breakdown process takes time to build up and depends on the laser field strength. It exhibits a threshold behavior, i.e., at a given laser pulsewidth, only when the laser field strength exceeds a certain threshold can the plasma density grow to the critical value where irreversible breakdown takes place. The threshold is customarily expressed as a laser fluence threshold as a function of pulsewidth.

Once the plasma of free electrons generated by avalanche ionization reaches a high enough density, irreversible material breakdown and ablation begin. The electrons absorb laser energy by collisions with ions and are heated to high temperatures. At the same time, the electrons transfer energy to the ions and the lattice, and the material is heated up. The amount of energy transfer, hence the heating, during the laser pulse depends on the pulse duration and the energy coupling

coefficient. When melting or vaporization temperature is reached, the material is considered broken down and damaged. The breakdown is also accompanied by acoustic waves and optical plasma radiation. The rate of heating is determined by the rate of laser energy absorption and the rate of energy loss from the focus, mainly through thermal conduction away from the focus. The rate of laser energy absorption is approximately constant before the breakdown.

## 2.2 Nanoparticles generated by laser ablation

A schematic representation of the plume generation and the subsequent generation of nanoparticles is shown in **Figure 2-3**.

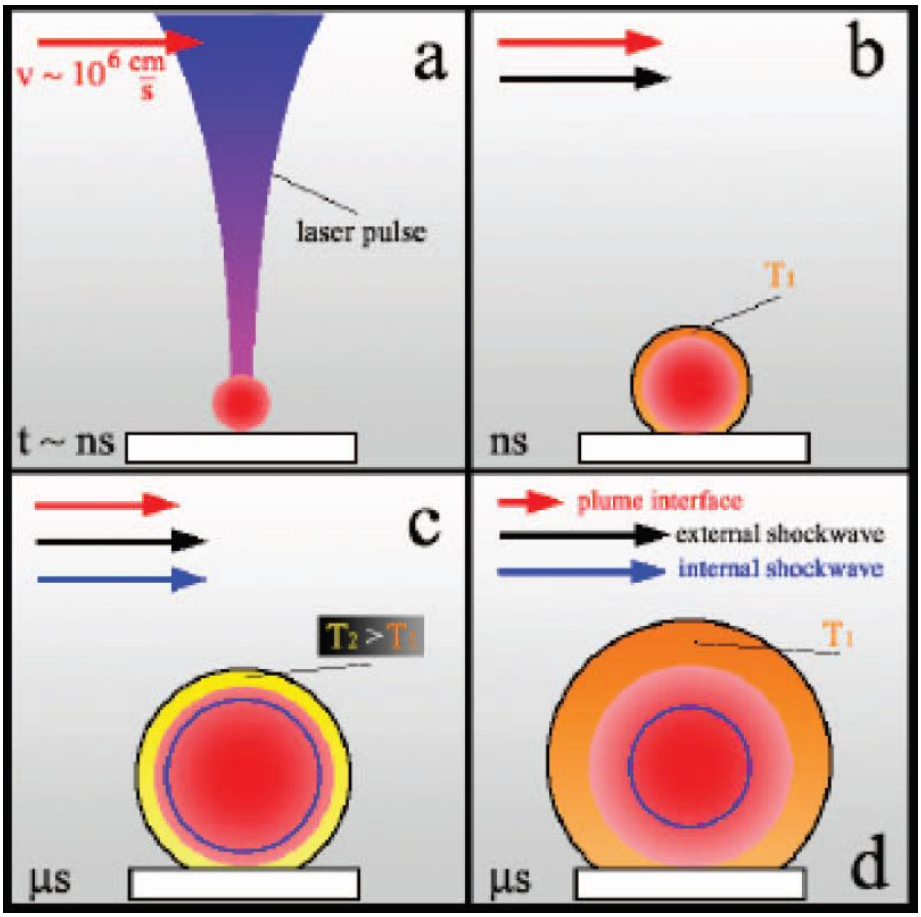


Figure 2-3: Schematic representation of plume generation by laser ablation [30]

The incidence of the laser beam on the material surface delivers an enormous amount of power to a small region of the material. This concentration of energy onto such a small region results in the ejection of material from the surface as highly energetic species in the form of a dense plume. The plume expands adiabatically, compressing the surround environment (background gas or air). The interaction between the plume and the gas result in the generation of a shockwave at the interaction interface. As the plume expands, the plume species lose their energy at the interface resulting in the formation of a pressure gradient. The pressure gradient creates an internal shockwave that travels towards the centre of the plume. As the laser pulses stop hitting the target, the plume cools down resulting in the condensation, nucleation and clustering of the plume species. This results in the formation of nanoparticles.

The mechanism discussed above gives a general insight into the generation mechanism of nanoparticles by laser ablation. However there are some fundamental differences in case of ultrashort pulse laser ablation and short/long pulse laser ablation. In case of ultrashort pulse laser ablation, the nanoparticles are ejected directly from the material surface through photomechanical effects. The ultrashort pulses result in superfast heating of the material and its conversion to a super-heated fluid accompanied with a build-up of extreme pressure. This leads to the ejection of the material from the surface of the target.

## 2.3 Summary

The advent of the laser technology opened new avenues for material processing. The laser ablation process provided an efficient method for micromachining of materials. Apart from

micromachining, the laser ablation process has been used for the generation of nanoparticles from a large range of materials. The mechanism for the removal of material through the ablation process has been mentioned as the heating of the material to above its critical point leading to the ejection of material from the top surface of the material. The ultrashort laser pulses have been found to be more effective in material removal through ablation in comparison with short/long laser pulses.

# Chapter 3: Experimental Method

## 3.1 Experimental Set-up

Experiments were conducted using a direct-diode-pumped Yb-doped fiber oscillator/amplifier femtosecond laser system capable of delivering a maximum output power of 16 W at a repetition rate of 26 MHz. The laser central wavelength is 1030 nm and pulse duration of 214 fs. The laser beam was focused into a spot of 10 μm using a telecentric lens of 100 mm effective focal length. A quarter waveplate was aligned with the beam expansion to obtain circular polarization. A galvoscanner was used for high speed beam positioning in x-y axis. An acousto-optic modulator was used as an optical shutter. A two-axis precision translation stage with a smallest resolution of 1 mm and a range of 15 cm is used to locate the laser irradiation spot on the sample surface. The pulse repetition rate varied from 2 MHz to 26 MHz. Figure 3-1 gives the schematic representation of the experimental setup.

## 3.2 Sample Preparation

Under the extent of the thesis, microparticle containing powders of nickel oxide (NiO), lead oxide ($Pb_3O_4$), zinc oxide (ZnO) and aluminum (Al) were used; the size of the particles was in the range of 10μm to 50μm. For studying the feasibility of the LAM process for the generation of a 3D nanostructure, the microparticle powders of NiO, $Pb_3O_4$ and ZnO were ablated. The microparticles of the oxide samples were glued onto glass slides; a layer of glue was applied onto the glass slide and a very fine layer of the microparticle containing powder was sprayed to form a fine layer of the powder on the glass slide. While preparing the sample, care was taken to

maintain a uniform thickness of the layer of the microparticles. The glass slide was chosen as the substrate as it was transparent and would not itself be ablated during the ablation of the microparticle layer. Glue which was transparent after drying was used for the adhesion process.

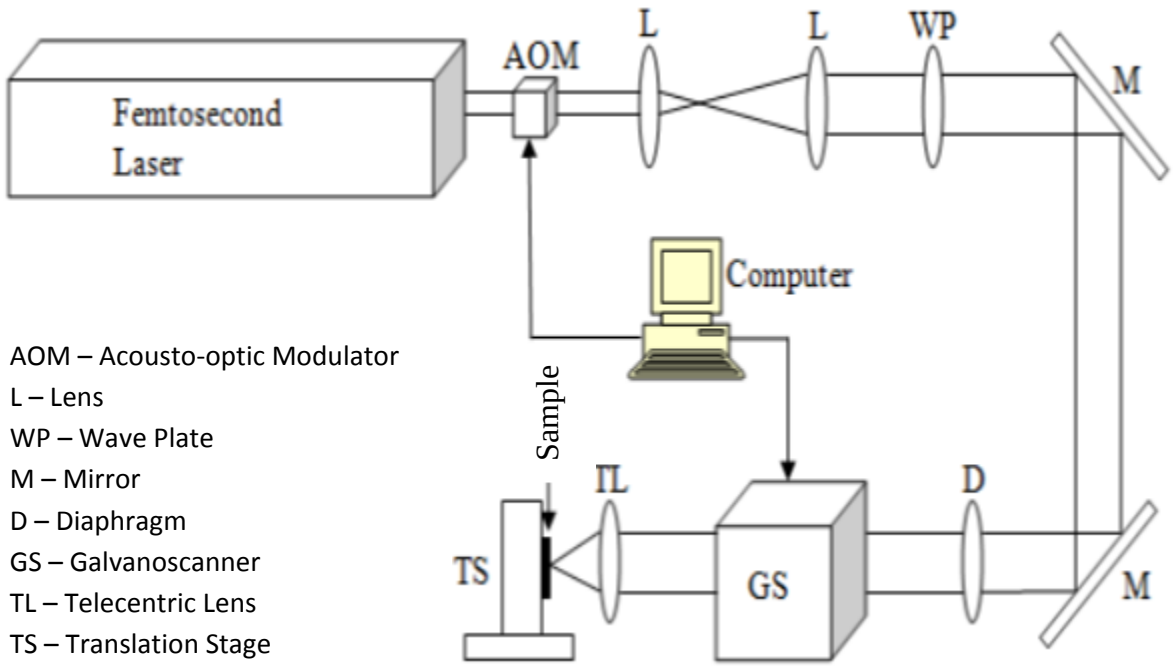


Figure 3-1: Schematic of the experimental set-up

The glue was later shown in the analysis to not have any effect on the generated nanostructure. Figure 3-2 shows an SEM image of the prepared microparticle layer. The samples were ablated at the laser power of 16W, with a repetition rate of 25MHz and a dwell time of 0.1ms.

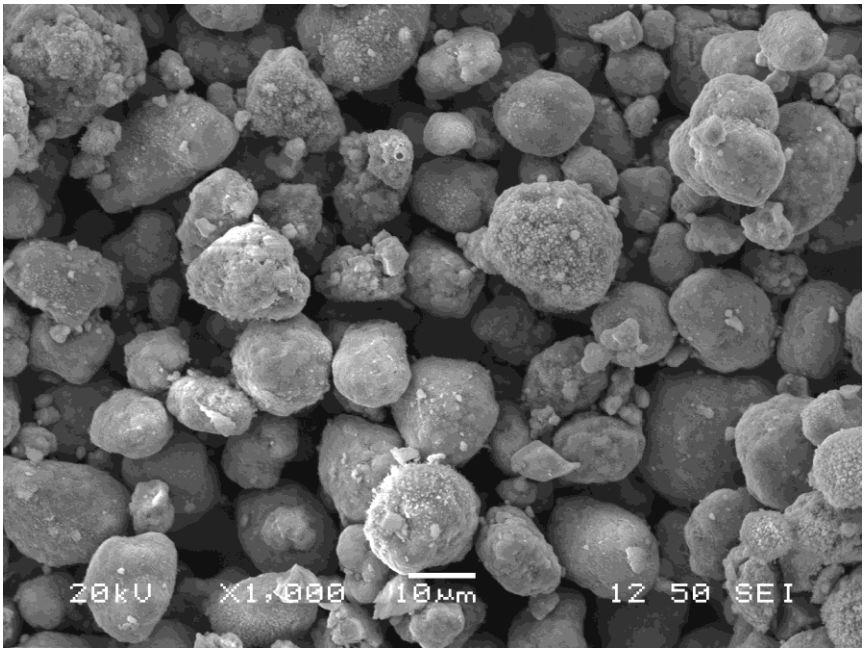


Figure 3-2: SEM image of the prepared microparticle layer of lead oxide ($Pb_3O_4$)

To analyse the mixing of two individual metallic microparticle species, microparticles of Al and NiO were used. The microparticle powders were taken and pre-mixed in a 1:1 ratio (by volume) by creating an aqueous mixture in isopropanol and subjecting the mixture to supersonic vibrations. The aqueous solution was then exposed to air to evaporate the isopropanol. The obtained mixture of the microparticle powders was glued onto a silicon substrate. The silicon substrate was chosen as it made for a better SEM analysis background (did not show as much charging as the glass substrate). The samples were ablated at a laser power of 12W, repetition rate of 8MHz and dwell time 0.25ms. In another experiment, the probability of mixing between the microparticles and a solid target was analysed. For this experiment, an aluminum foil was glued onto a glass slide. A layer of the glue was applied to the foil surface and the microparticles of NiO sprayed on it.

## 3.3 Sample Analysis

The ablated samples were analyzed for the nanostructure generated. The morphology was analyzed using a SEM (Hitachi S-5200 SEM) and a Transmission Electron Microscope (TEM) (Hitachi HD-2000 STEM). X-Ray Diffraction (XRD) analysis was also carried out on the ablated and non-ablated samples of lead oxide ($Pb_3O_4$) and nickel oxide (NiO), to confirm that the stoichiometry was maintained during the ablation process. Energy Dispersive X-Ray (EDX) analysis was carried out to determine the elements present in the generated nanostructures.

# Chapter 4: Femtosecond laser ablation of metallic microparticles

## 4.1 Introduction

Earlier research conducted at the Laser Micro and Nano Fabrication Research Facility at Ryerson University showed that the use of megahertz laser ablation can generate fibrous nanoparticle networks from metals, dielectrics and a wide range of other material [31-33]. A lot of research has been focused on the generation of nano-networks through laser ablation of bulk substrates. The mechanism behind the generation of nano-networks through laser ablation has been found to be the agglomeration of the nanoparticles that are generate by the ablation of the substrate. Thus the size of the generated nano-network is dependent on the size of the agglomerated nanoparticles.

In this chapter, the study on the generation of very fine nanoparticle networks by the process of laser ablation of microparticles will be discussed. The results of the laser ablation of microparticle sample will be presented. The observed results will be compared with similar results obtained through laser ablation of bulk material. Also discussed in this chapter is the proposed mechanism for the reduction in size of the nanoparticles leading to the formation of very fine nanoparticle networks.

## 4.2 Experimental Parameters

The sample preparation methods are mentioned in Section 3.2. The prepared samples were ablated in an ambient air using a Yb-doped fiber amplified femtosecond laser. The ablation of all the samples was carried out with the same laser parameters. The laser parameters were set as follows:

- Average power per pulse: 16W
- Repitition rate: 25MHz
- Dwell time: 0.1ms

## 4.3 Results and Observations

Figure 4-1 shows the SEM image of the 3D nanoparticle networks generated in an ablated sample of lead oxide ($Pb_3O_4$) microparticles. More images of the nanoparticle networks generated by the laser ablation of microparticles are included in the appendix. Appendix A shows the SEM images of the nanoparticle network obtained by ablation of microparticles of Lead Oxide ($Pb_3O_4$). Appendix B shows the SEM images of the nanoparticle network obtained by ablation of microparticles of Nickel Oxide (NiO). Appendix C shows the SEM images of the nanoparticle network obtained by ablation of microparticles of Zinc Oxide (ZnO).

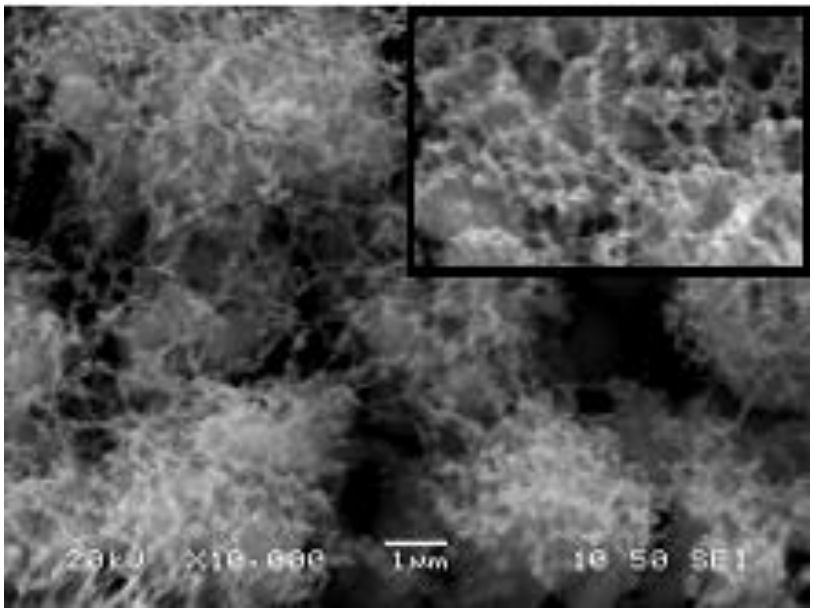


Figure 4-1: Nanoparticle network growth in ablated Lead Oxide microparticles
(Insert: Magnified image of nanostructure)

In the traditional LAM process, the ablation process leads to the formation of nanoparticles only. A possible explanation for this is that the photo-ionization of the formed nanoparticles (due to the longer pulse duration of the nanosecond laser) prevented the agglomeration of the nanoparticles [26]. In the current experiment, the ultrashort pulse duration of the femtosecond laser does not provide enough time for the particles to be photo-ionized. Hence the generated nanoparticles agglomerate to form nanofibers. Thus the LAM process has been successfully used for the generation of nanofibers from microparticles.

A comparison was carried out between the laser ablation of the microparticle containing sample and those generated through ablation of bulk lead sample. The first noticeable difference was the change in the threshold fluence for the initiation of ablation of the sample. The threshold fluence for the microparticle sample was calculated to be $0.0815 J/cm^2$. While the threshold fluence for the bulk lead sample was determined to be $0.285 J/cm^2$. The threshold fluence for the ablation of

the microparticle containing sample was 3.5 times less than the fluence for the ablation of the bulk substrate sample.

The nanoparticle networks generated by LAM were compared to those generated by ablation of solid substrate. The comparison was carried out for the lead sample. The compared results are shown in the Figure 4-2, where the nanoparticle networks formed by ablation of microparticles of lead oxide are compared with the similar networks formed by the ablation of a solid target of bulk lead.

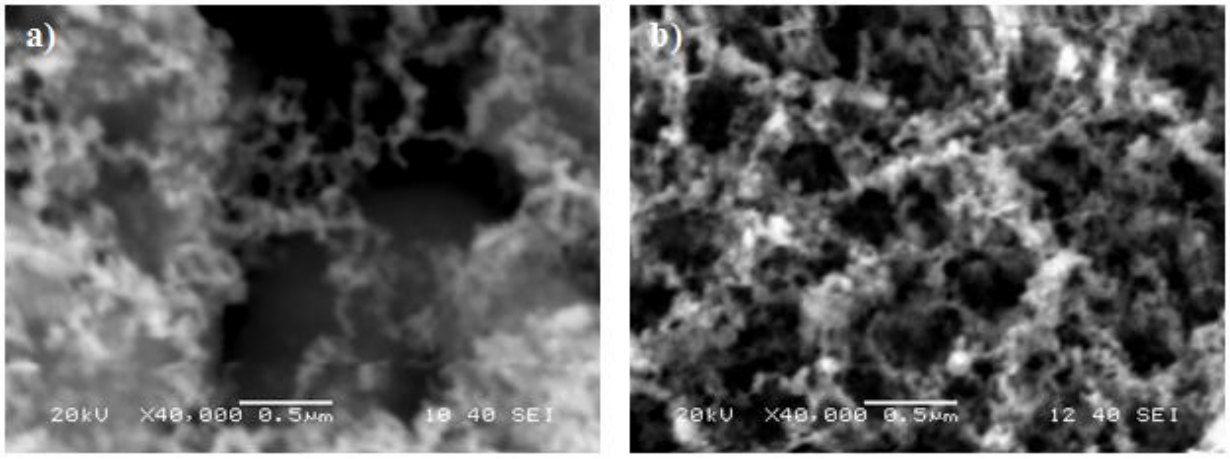


Figure 4-2: Nanoparticle networks formed by ablation of: a) microparticles of lead oxide, b) bulk lead

By comparing the nanoparticle networks from the two samples, there was found to be a difference in the size of the nanoparticle networks generated. The nanoparticle networks generated by the ablation of the solid substrate had a diameter in the range of 110-160nm. The diameter of the nanoparticle networks generated by the LAM process ranged from 60nm to 90nm. There is a considerable shift in the diameter of the nanoparticle networks for the two samples though the same laser parameters were used for the two experiments.

A size distribution analysis of the bulk and microparticle sample was carried out. The result of the distribution analysis is as shown in the Figure 4-3. From the table it can be seen that the size of the generated nanoparticle structure for the microparticle sample is concentrated in the 60nm - 70nm range. While in the case of the bulk sample, the size ranges from 100nm – 160nm with its peak at 130nm size.

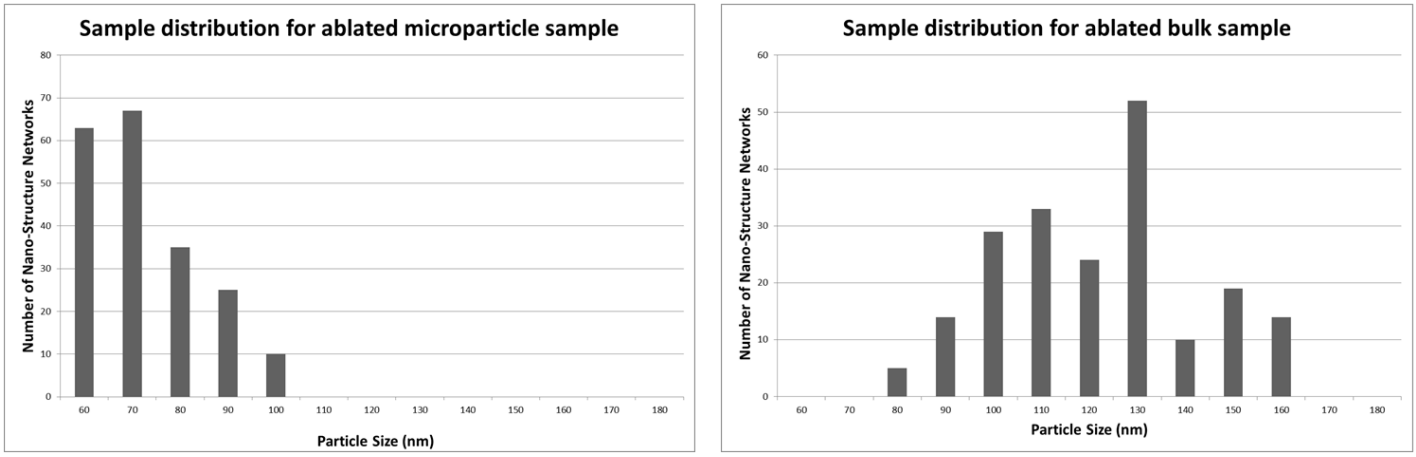


Figure 4-3: Size distribution for the microparticle sample and the bulk sample

## 4.4 Discussion

The formation of the nanoparticle networks has been attributed to the agglomeration of the nanoparticles generated by the laser ablation of the microparticles. Hence the shift in the diameter of the nanoparticle networks can be explained by the shift in the size of the generated nanoparticles.

The explanation for the reduction of the nanoparticle size is obtained by analyzing the shockwave generated by the laser ablation process. One of the characteristics of the LAM

process is the concentration of the generated shockwave onto a smaller volume of the particles [28]. A schematic for the generation of shockwave and its propagation is shown in Figure 4-4.

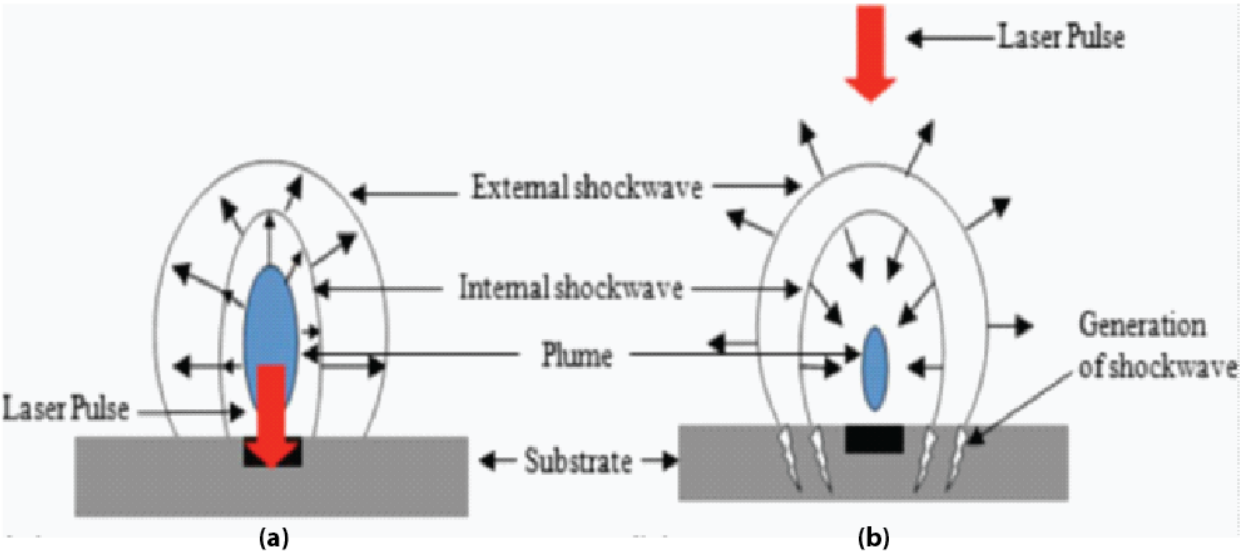


Figure 4-4: Schematic representation of the shockwave generated by laser ablation [34]

After the ablation of the microparticles, two shockwaves are generated; an external shockwave and an internal shockwave as shown in Figure 4-4a. As the shockwaves expand into the background atmosphere, the external shockwave is slowed down. The faster travelling internal shockwave gets reflected off the slower moving external shockwave and travels towards the sample; shown in Figure 4-4b. The shockwave travelling into the sample creates a region of low pressure as it passes. Catastrophic condensation occurs in the low pressure region leading to the breakdown of the microparticles into nanoparticles [28, 34, 35]; the size of which is much smaller than that of the nanoparticles produced by the laser ablation of a bulk substrate.

The XRD analysis of the ablated and the non-ablated sample was carried out to ascertain that the chemical composition of the two was maintained through the experiment. The result of the XRD

analysis on lead oxide ($Pb_3O_4$) sample pre- and post-ablation has been shown below. The XRD analysis result for nickel oxide (NiO) is included in Appendix D.

Note: For the graphs shown in Figure 4-5 and Figure 4-6, there is a difference in the value obtained for intensity (measured in counts per second (cps)). This difference in the intensity does not imply a change in the stoichiometry of the material before and after ablation. The intensity value is dependent on the signal picked up by the sensor. The location of the peaks in the two graphs at precisely the same point indicates the uniformity of chemical composition.

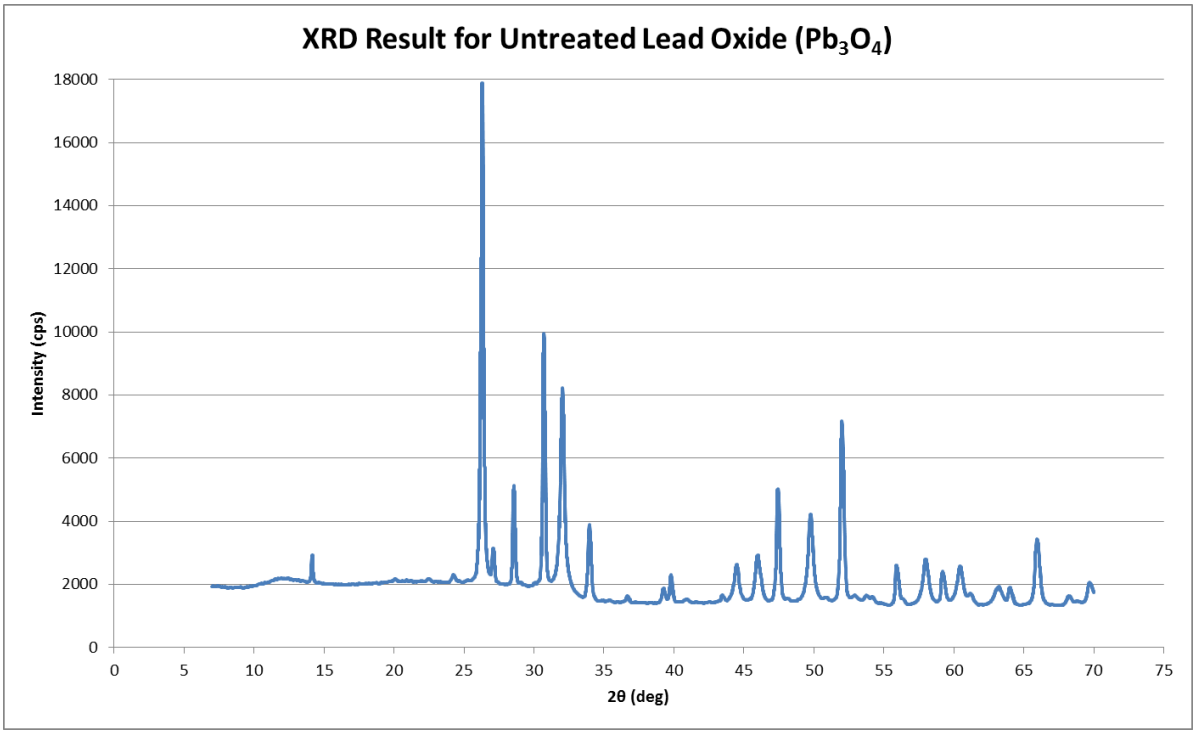


Figure 4-5: XRD graph for non-ablated sample of $Pb_3O_4$ microparticles

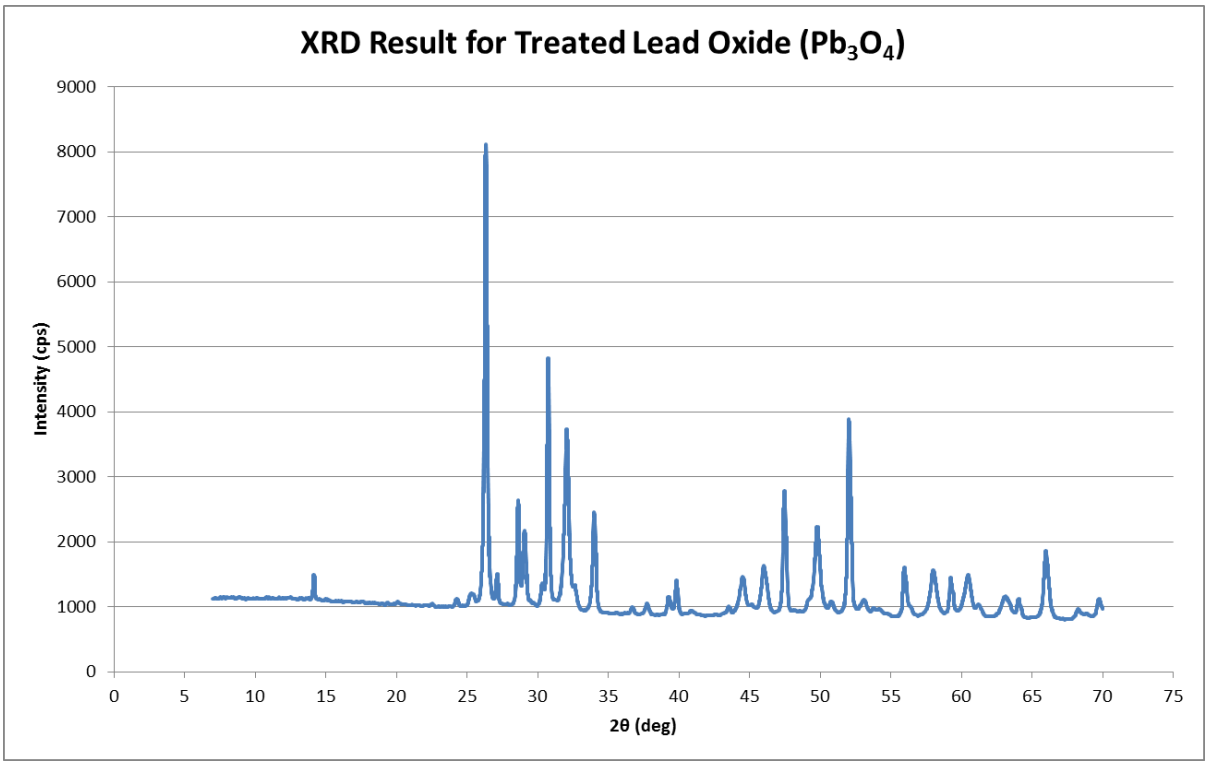


Figure 4-6: XRD graph for $Pb_3O_4$ microparticle sample post ablation

To further ascertain the claim that the stoichiometry is maintained after ablation, the XRD data obtained for the ablated sample of lead oxide was compared with the XRD data for lead oxide found in the database (JCPDS file number 89-1947). The two data were in close agreement with each other; indicating that the beginning sample and the end product were of the same chemical composition. The similarity between the two data's suggests that the polymer contained in the glue has completely been vaporised by the interaction of the laser and hence does not interfere in the process of formation of the nanoparticle networks under investigation. A few extra peaks were observed during the comparison; these could be explained by considering the fact that the sample might have come in contact with some contaminants.

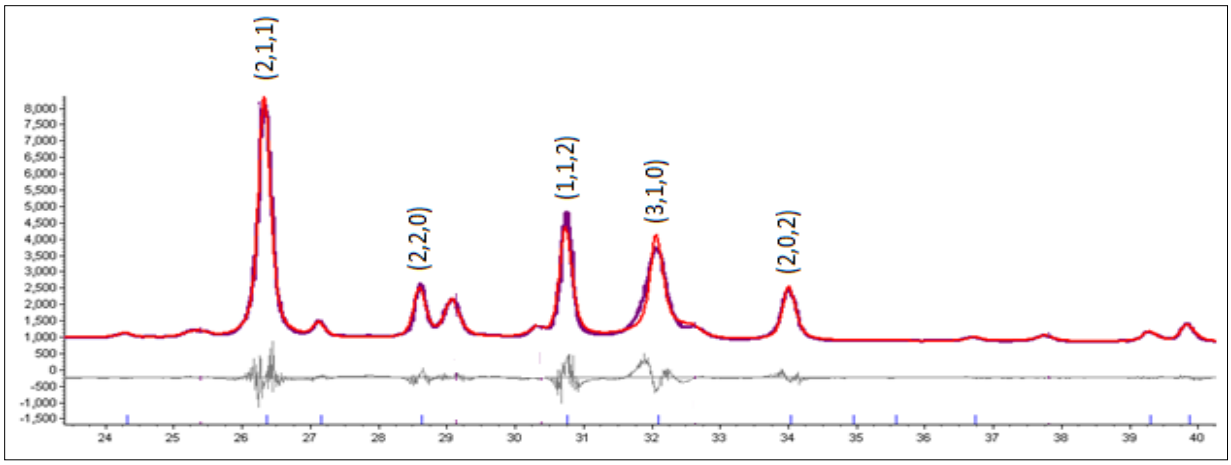


Figure 4-7: Comparison of obtained and standard data for Lead Oxide; also shown are the prominent phases

In Figure 4-7, a graph for the XRD data of the ablated lead oxide microparticle sample was superimposed onto the graph for lead oxide from the International Centre for Diffraction Data's database. The two graphs completely overlapped each other. The noise component is seen as the gray line. The prominent phases that were obtained are also shown in Figure 4-7; these peaks coincided with the peaks that were expected for a sample containing lead oxide ($Pb_3O_4$).

## 4.5 Conclusion

A new approach towards the generation of 3D nanoparticle networks has been presented in this study. Microparticle containing samples were ablated using a femtosecond laser and nanoparticle networks with a sub-100nm nanoparticle size range were observed. On comparison with the similar nanoparticle networks obtained through ablation of bulk material, a reduction of approximately 60nm in the size of the nanoparticles was observed. The reduction in size has been attributed to the propagation of the generated shockwave through the loosely packed

microparticles. Another significant observation was a 3.5 times drop in the ablation threshold fluence for the microparticles in comparison to the bulk sample of the same material.

This study has shown that femtosecond laser ablation in an ambient environment can be used for generating a 3D nanoparticle network from microparticles without the use of external stimulants or catalysts. The technique thus presented can be used for efficient generation of nanoparticle networks from a vast array of materials without the use of toxic or hazardous chemical precursors.

# Chapter 5: 3D nanostructure through laser ablation of mixture of Al and NiO microparticles

## 5.1 Introduction

Properties of materials have been shown to be different at the nano scale in comparison to the properties at the macro scale. Therefore, to utilize the advanced properties at the nano scale numerous methods have been developed for the generation of nanoparticles from a vast variety of materials. Nanoparticles generated from individual precursor materials (metals, polymers, semiconductors, dielectrics) have been shown to be useful for a lot of applications [25, 36-38]. However, one realm of nanoparticles that has not been studied is capitalization of the advanced properties of a group of nanoparticles in a combination to achieve a new material/alloy with properties superior to those of the nanoparticles of the individual materials.

Over the years, non-conventional methods have been used for the synthesis of nanocrystalline alloys from immiscible metals. Methods such as ion beam mixing, sputtering, vapor deposition, thermal evaporation and laser ionization have been used for the synthesis of such alloys [39-43]. All these non-conventional methods take advantage of the theoretical predictions of lowered or suppressed phase separation at the nano scale [44, 45]. One theory has suggested the lack of nucleation barrier for the formation of segregated species at the nanoparticle size regime [46].

Some effort has been made to produce such nanoparticle alloys through laser ablation of colloidal solutions or powder suspensions of materials [47-51]. In all of these methods some kind of liquid solution of the materials is irradiated with the laser to generate the nanoparticles which

are a combination of the materials either in the form of a core-shell structure or a metastable alloy. These methods are limited by the preparation of such a liquid solution of the mixing materials.

In the previous chapter, the generation of a 3D nanostructure upon ablation of a microparticle containing powder has been demonstrated [52]. This chapter studies the use of the ablation process presented in the previous chapter to generate a 3D nanostructure composed of a mixture of two materials that initially do not exist in a combined form. The generation of a 3D nanostructure by the laser ablation of a mixture of Nickel Oxide (NiO) and Aluminum (Al) microparticle powders is presented. In extension to the above results, also reported is the generation of 3D nanostructure through ablation of Nickel Oxide (NiO) powder layer on an Aluminum foil; the generated nanostructure shows a different type of material.

## 5.2 Experimental Parameters

The sample preparation methods are mentioned in Section 3.2. The prepared samples were ablated in an ambient air using a Yb-doped fiber amplified femtosecond laser. The ablation of all the samples was carried out with the same laser parameters. The laser parameters were set as follows:

- Average power per pulse: 12W
- Repitition rate: 8MHz
- Dwell time: 0.25ms

## 5.3 Results and Discussion

For the current study, a mixture of two microparticle containing powders was ablated and the nanostructure generated was analyzed. Figure 5-1 shows an illustrative depiction of the ablation process and the corresponding nanostructure generated.

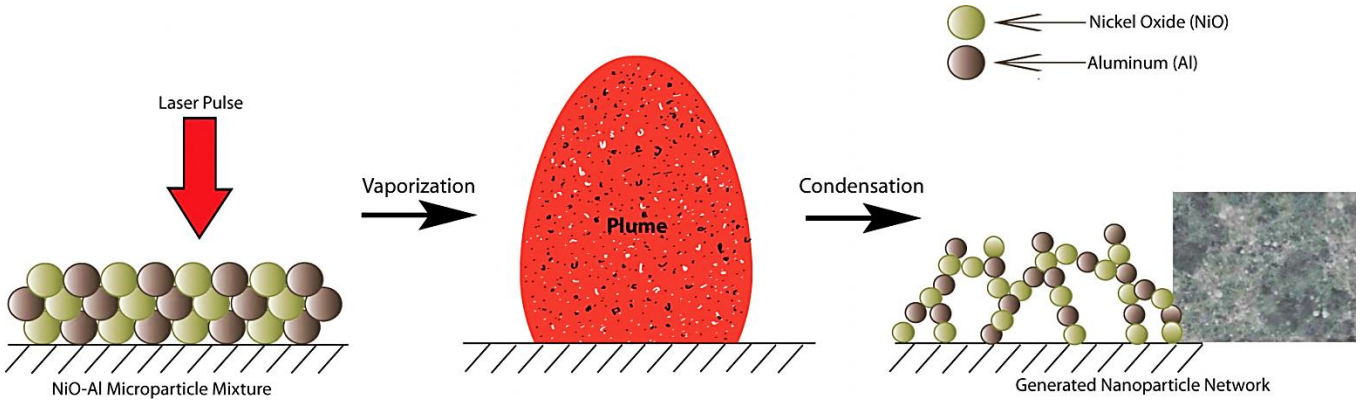


Figure 5-1: Laser ablation of a mixture of two microparticle containing powders

The ablated samples were analyzed under the SEM to study the generated nanostructure. Figure 5-2 shows the SEM images of the nanostructure generated by the laser ablation of a mixture of aluminum and nickel oxide microparticles.

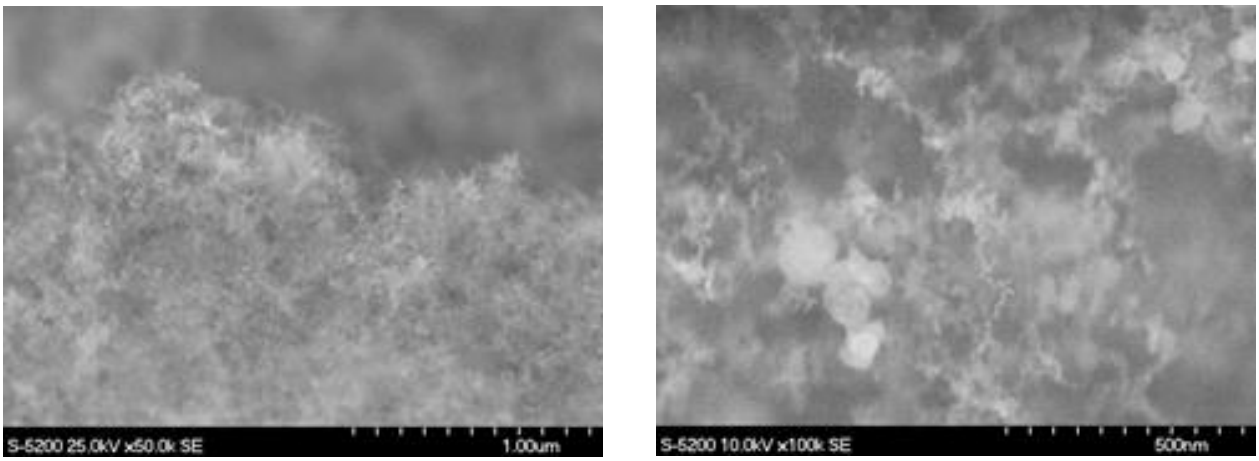


Figure 5-2: SEM image of generated microstructure

From Figure 5-2, it can be seen that the structure of the generated nanostructure is similar to the nanostructure obtained in the previous work. The EDX analysis confirmed the presence of both aluminum and nickel in the obtained nanostructure. Figure 5-3 presents the result of the EDX analysis carried on the sample.

On a closer examination of the TEM images, two types of mixing were observed:

1. Nanoparticles fused to form 3D nanostructures (Figure 5-4)
2. Aluminum particles embedded in nickel nuclei (Figure 5-5)

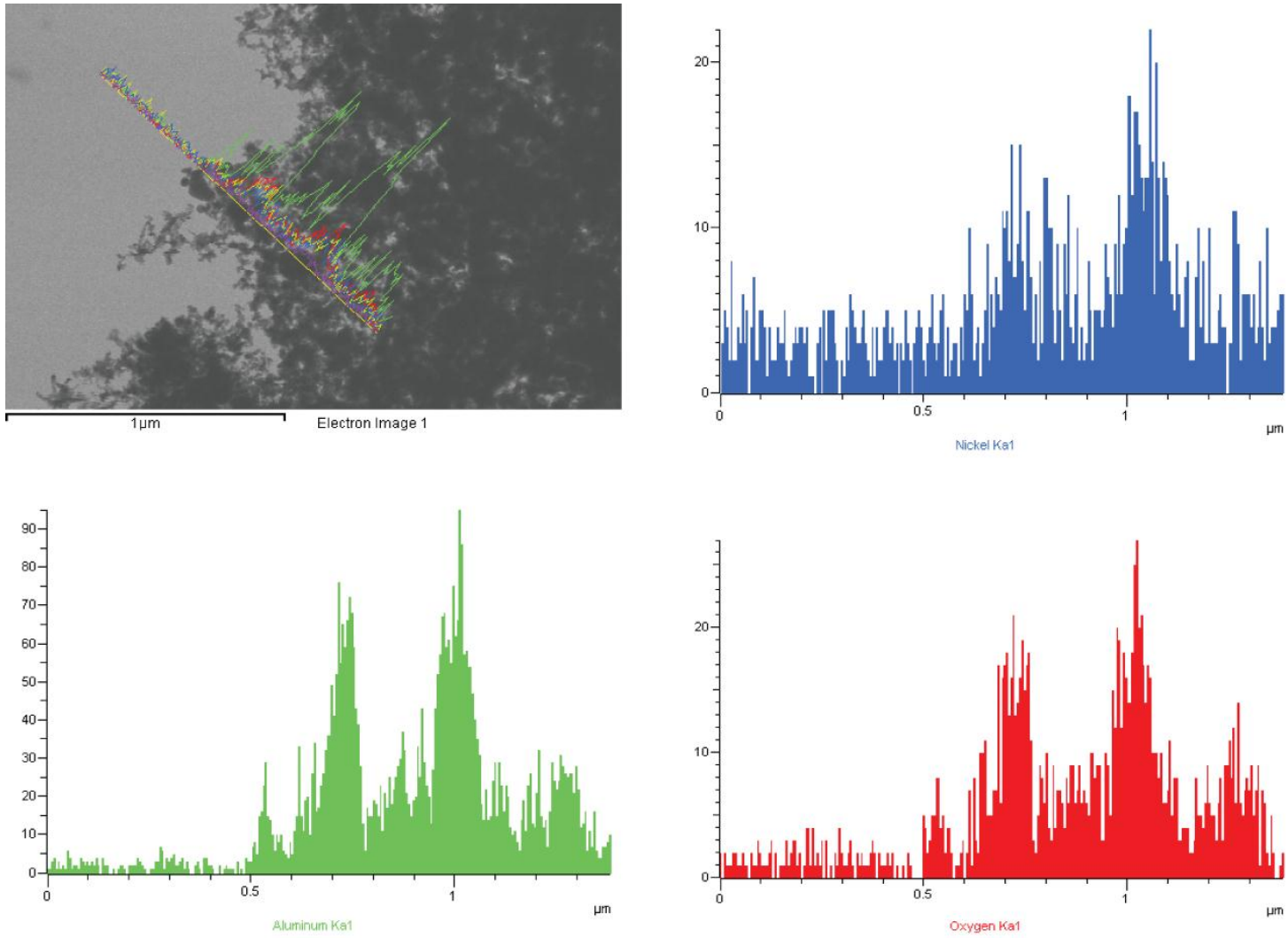


Figure 5-3: EDX analysis result confirming presence of Al and Ni in the nanostructure

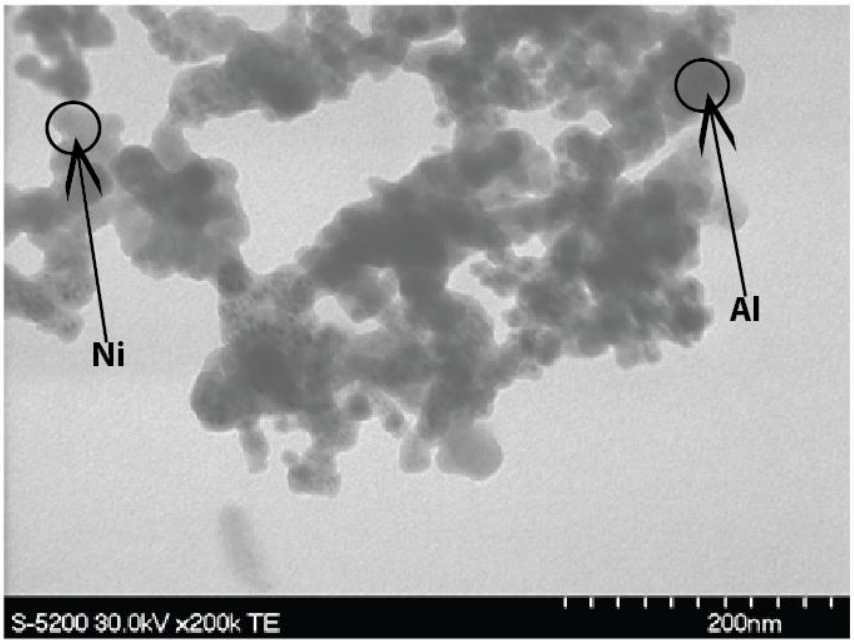


Figure 5-4: TEM image of the generated nanoparticle network

In order to explain the post ablation mixing of the two powders, the fundamental behind the process of laser ablation for material removal has to be re-looked into. The method of material removal by laser ablation has been explained by the heating of the target material above its boiling temperature by the laser pulses, followed by rapid cooling once the laser pulses stop. When ablation of the target material is carried out in a background gas environment or in ambient air, the presence of the air/gas causes the re-deposition of the ablated material onto the target surface which does not take place for laser ablation in vacuum [53].

In the current study, the technique demonstrated in the previous work (laser ablation of microparticles for generating a nanoparticle network) has been used for the ablation of a mixture of Nickel Oxide and Aluminum powders. Due to presence of two powders of two different chemical compositions, there is a difference in the boiling point of the two. This difference in the

boiling point becomes a factor during the cooling phase that follows after the laser pulses have stopped hitting the target. As per the material data for aluminum and nickel oxide, there is a huge gap in the boiling point temperature for the two materials. Nickel has a higher boiling point temperature (2730$^{o}$C) than aluminum (2327$^{o}$C). Thus after the laser pulses stop, during the rapid cooling phase, the nickel oxide solidifies faster than aluminum. The cooled nickel oxide provides nucleation sites for the cooling aluminum. This results in the deposition of the aluminum nanoparticles on nickel oxide nuclei; clearly observed in the TEM image shown in Figure 5-5.

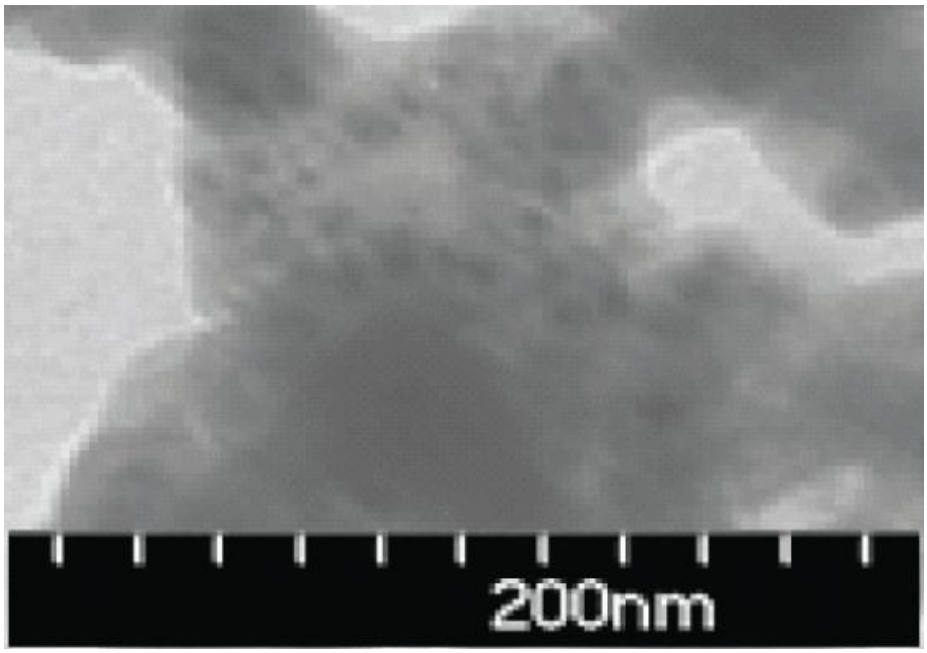


Figure 5-5: TEM image showing Al embedded in Ni nuclei

Another aspect of laser ablation that has been recently highlighted is the presence of a temperature gradient that exists across the surface of the target material [54]. The temperature at the point where the laser directly hits is the highest and it decreases as we move away from the center. There is also the existence of isotherms across the target surface [54]. Taking into

account the above temperature gradient, the layer of mixture of aluminum and nickel oxide powders will be subject to different temperatures depending on the position from the point of laser impact. Thus there exists a variation in the extent of mixing of the two powders post ablation. Figure 5-6 shows the TEM images of the nanostructure generated in the area away from direct impact of the laser.

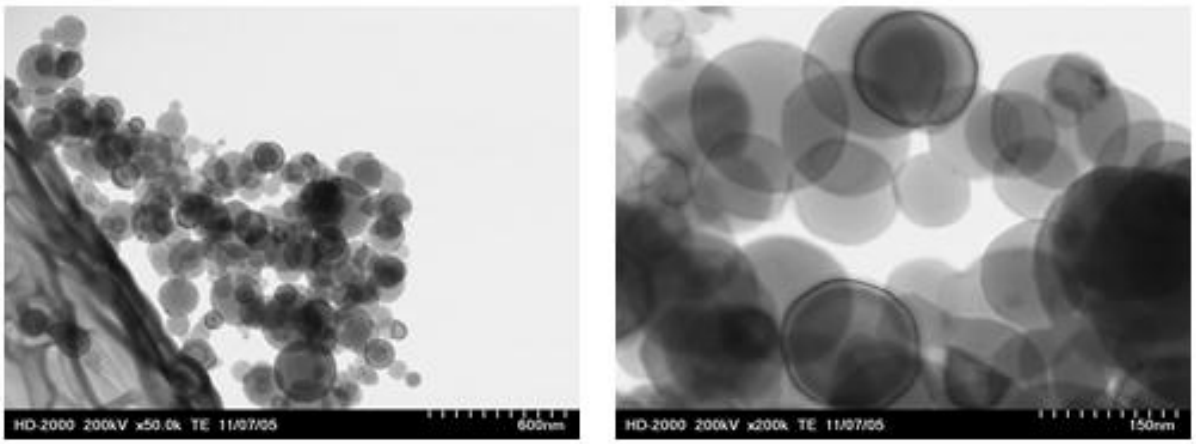


Figure 5-6: TEM images of the generated nanostructure

Figure 5-7 shows a closer comparison between the mixing at the centre and away from centre. The difference in the mixing becomes clearly visible in that in case of Figure 5-7a, the aluminum nanoparticles are embedded in a background of nickel while in Figure 5-7b aluminum and nickel oxide form interconnected chains and do not show signs of mixing between the two in the plasma state.

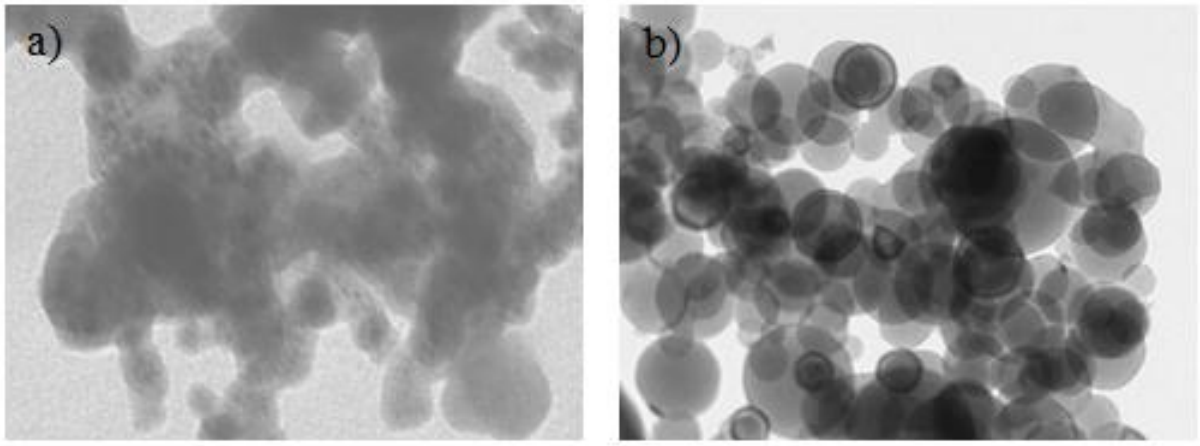


Figure 5-7: TEM images of bonding observed; a) at the center of laser impact, b) away from center

In extension of the above study, the microparticles of aluminum were replaced by an aluminum foil. A layer of the microparticles of nickel oxide was applied onto the aluminum foil. The sample was then ablated and analyzed for nanostructure generation. The process is illustrated in Figure 5-8.

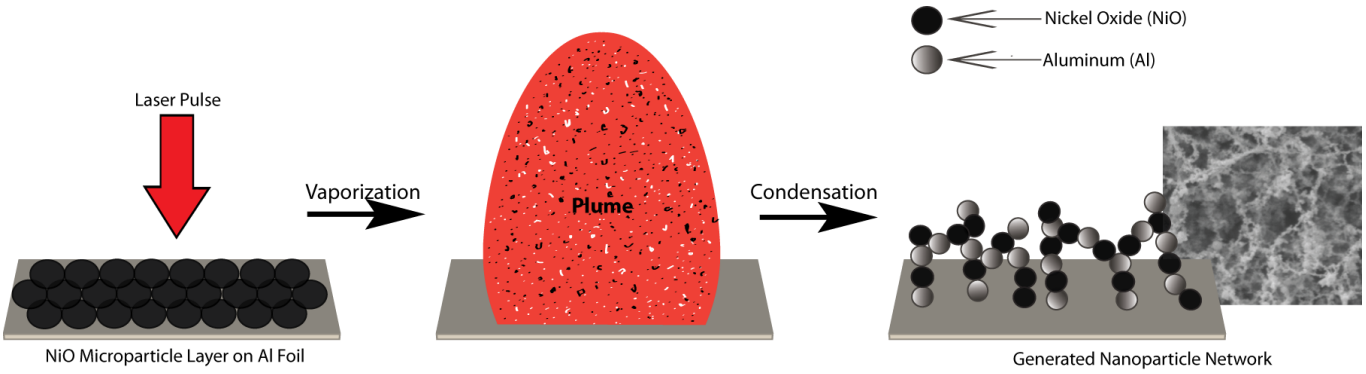


Figure 5-8: Laser ablation of NiO microparticle layer applied to an aluminum foil

For the current scenario, as shown in Figure 5-8, the laser was focused so as to ablate the microparticle layer and the aluminum foil simultaneously. The particles from the foil and the microparticle layer were ejected into the plume and upon subsiding of the laser pulses formed into nanoparticle networks. The generated networks showed certain extent of mixing between the

two materials. Figure 5-9 shows the SEM image of nanostructure obtained by the ablation of NiO microparticles coated on an Aluminum foil.

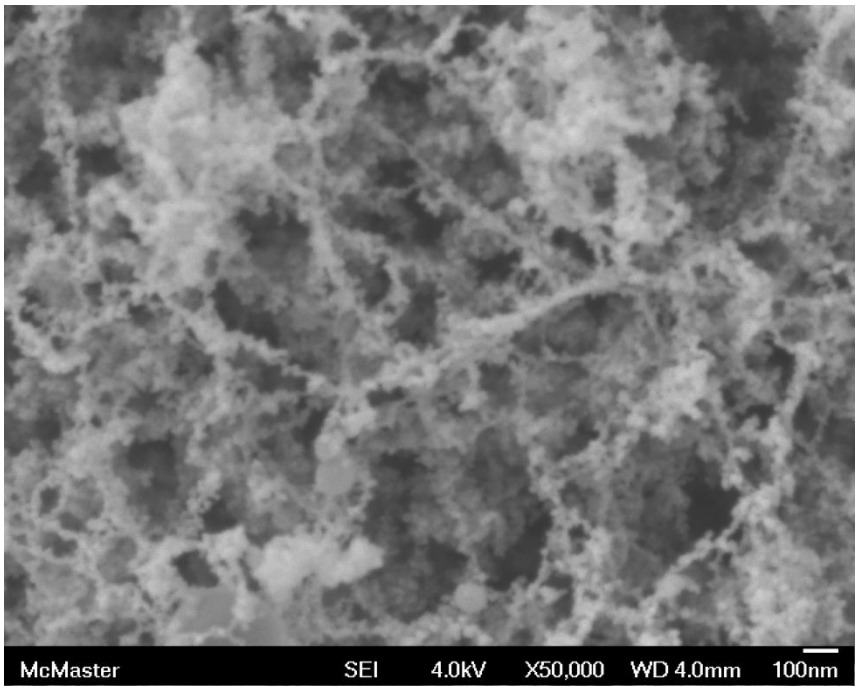


Figure 5-9: SEM image of nanostructure generated by laser ablation of NiO microparticles on Al foil

## 5.4 Conclusion

In the current study, the process of laser ablation of microparticle for generating a nanostructure (as described in Chapter 4) has been successfully applied for the generation of a 3D nanostructure through laser ablation of a mixture of aluminum and nickel oxide microparticle containing powders. Apart from the generation of the nanostructure, mixing between the two powders is also observed. Two different types of mixing are observed; one where aluminum is embedded in a pool of nickel oxide and the other where nickel and aluminum are present in an agglomerated chain of their nanoparticles. The mixing has been explained by the difference in

the boiling point of the two powders and its effect during the rapid cooling phase after the end of the laser pulse train. This study provides an alternative for the synthesis of alloy nanomaterial.

# Chapter 6: Conclusion and Future Work

## 6.1 Contributions

The main contributions of this research are:

- Synthesised self-assembled agglomerated nanoparticle networks by femtosecond laser ablation of microparticle samples.
- Generated nanoparticle agglomerates from microparticles by femtosecond laser ablation under ambient conditions; atmospheric conditions and without use of external catalysts or stimulants.
- Generated an alloy nanostructure by femtosecond ablation of two metallic microparticle powders.
- Demonstrated the use of femtosecond laser ablation for generating a nanostructure by ablation of two metals in different phases; one in microparticle powder form and the other in solid form.

## 6.2 Conclusion

Femtosecond laser ablation of bulk materials generates 3D nanoparticle networks when the laser pulse repetition rate is in the Mega Hertz (MHz) regime. The generated nanoparticles normally have diameters in the range of a few hundreds of nanometers. To further reduce the particle size, the process of laser ablation of microparticles (LAM); which has long been used for the generation of individual nanoparticles from microparticles, has been used for generating a 3D

nanoparticle network by using lead oxide ($Pb_3O_4$) microparticles, nickel oxide (NiO) microparticles and zinc oxide (ZnO) microparticles as precursors.

The increased efficiency of the LAM process for generating nanoparticle networks in comparison to laser ablation of bulk material was demonstrated with lead samples; wherein the size of the generated nanoparticles was approximately 60nm smaller than those generated from ablation of bulk lead. Reduced laser fluence for the LAM process; attributed to the loosely packed nature of the microparticles, provided for nanostructure generation at lowered laser energy level.

Apart from generation of nanostructure from microparticles of a single material, nanostructures were also obtained for ablation of a mixture of microparticle powders. The generated nanostructures showed mixing between the two microparticle materials (Al and NiO) during the ablation process; a fact highlighted by the EDX analysis. The difference in the boiling point of the two materials was proposed to be the cause of the mixing of NiO and Al during the condensation phase.

## 6.3 Suggestions for Future Works

The novel method of formation of an alloy nanoparticle network can be further expanded in various directions. The composition of the alloy obtained can be varied by changing the mixing ratio of the two powders. Also the effect of change in laser parameters can be studied. Research can also be carried out on the influence of the presence of a background gas on the alloy nanoparticle network obtained.

# Appendix

## Appendix A: Nanoparticle networks from $Pb_3O_4$ microparticles

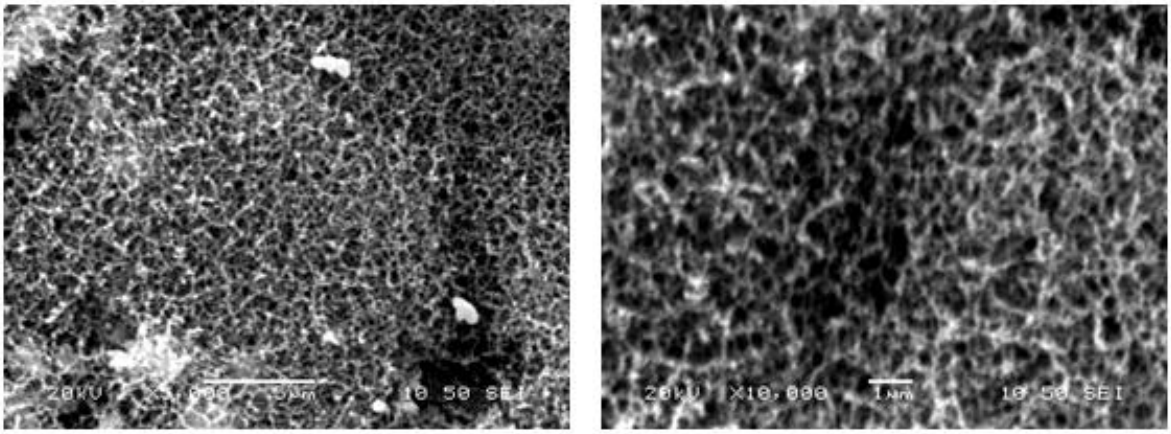


Figure A-1: Nanofibrous structures by ablation of $Pb_3O_4$ microparticles

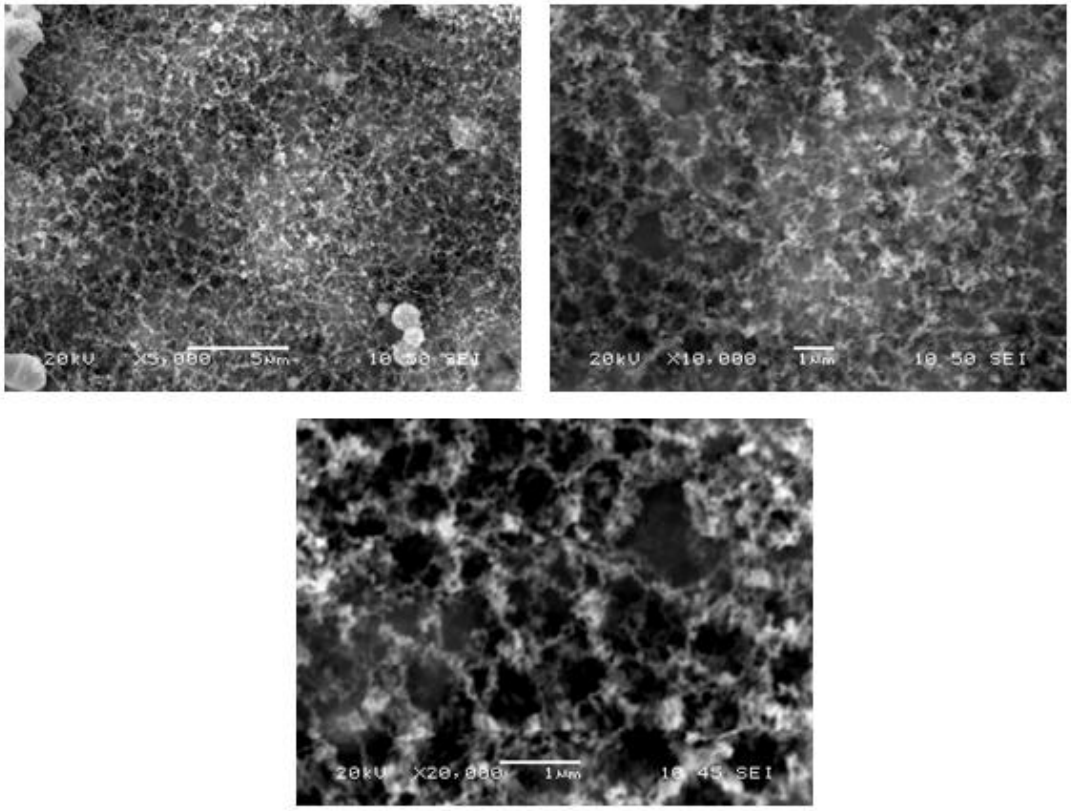


Figure A-2: Nanofibrous structures by ablation of $Pb_3O_4$ microparticles

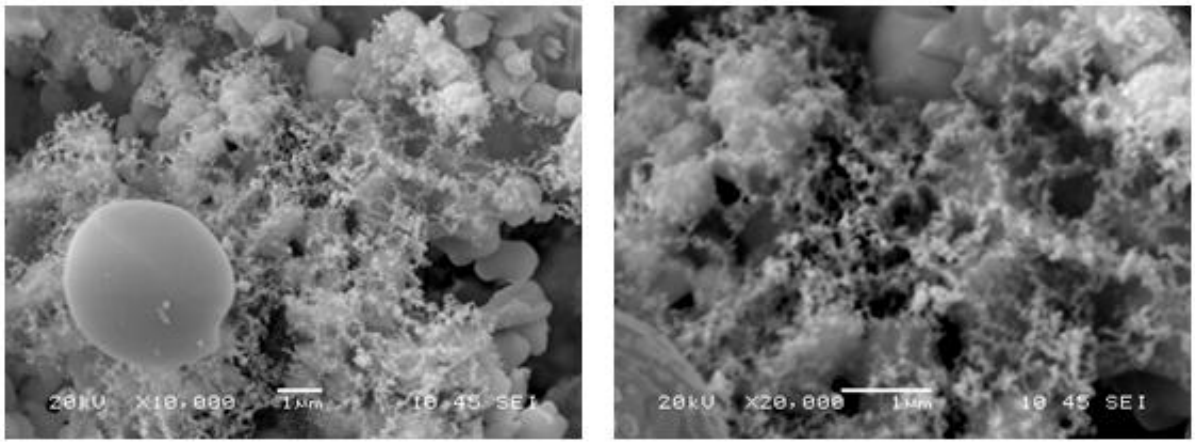


Figure A-3: Nanofibrous network growth on ablated microparticles

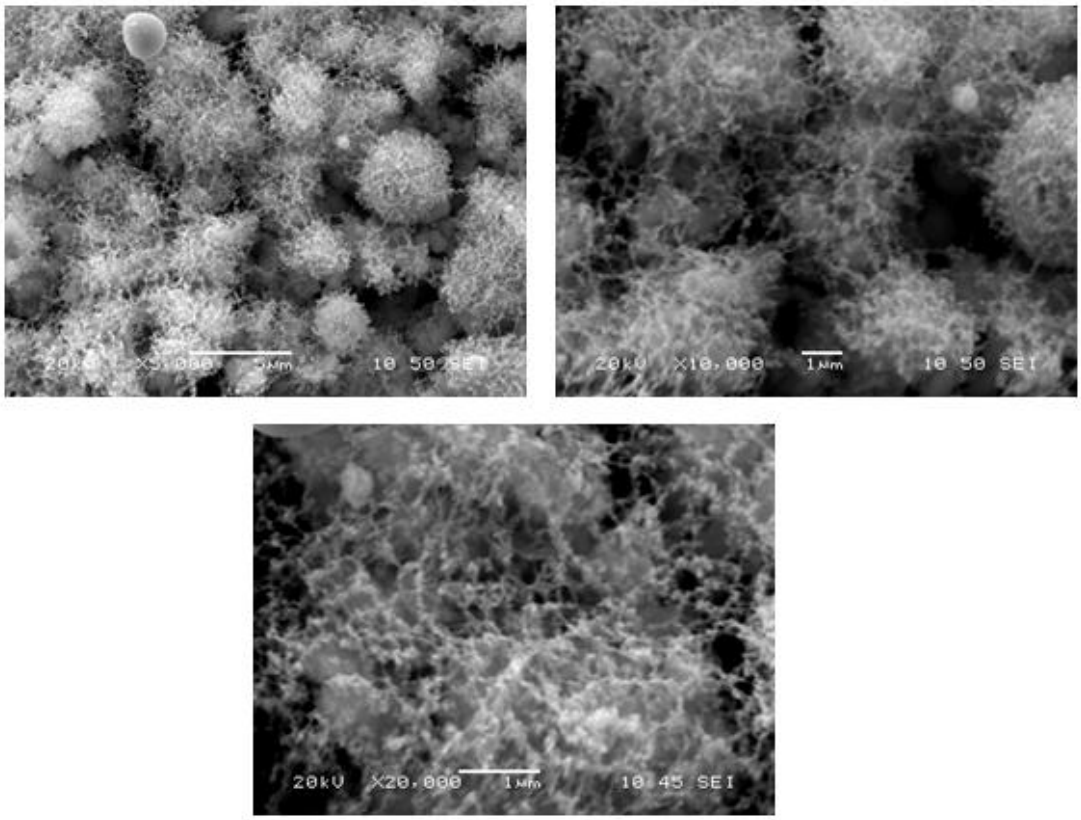


Figure A-4: Nanofibrous network growing from ablated microparticles

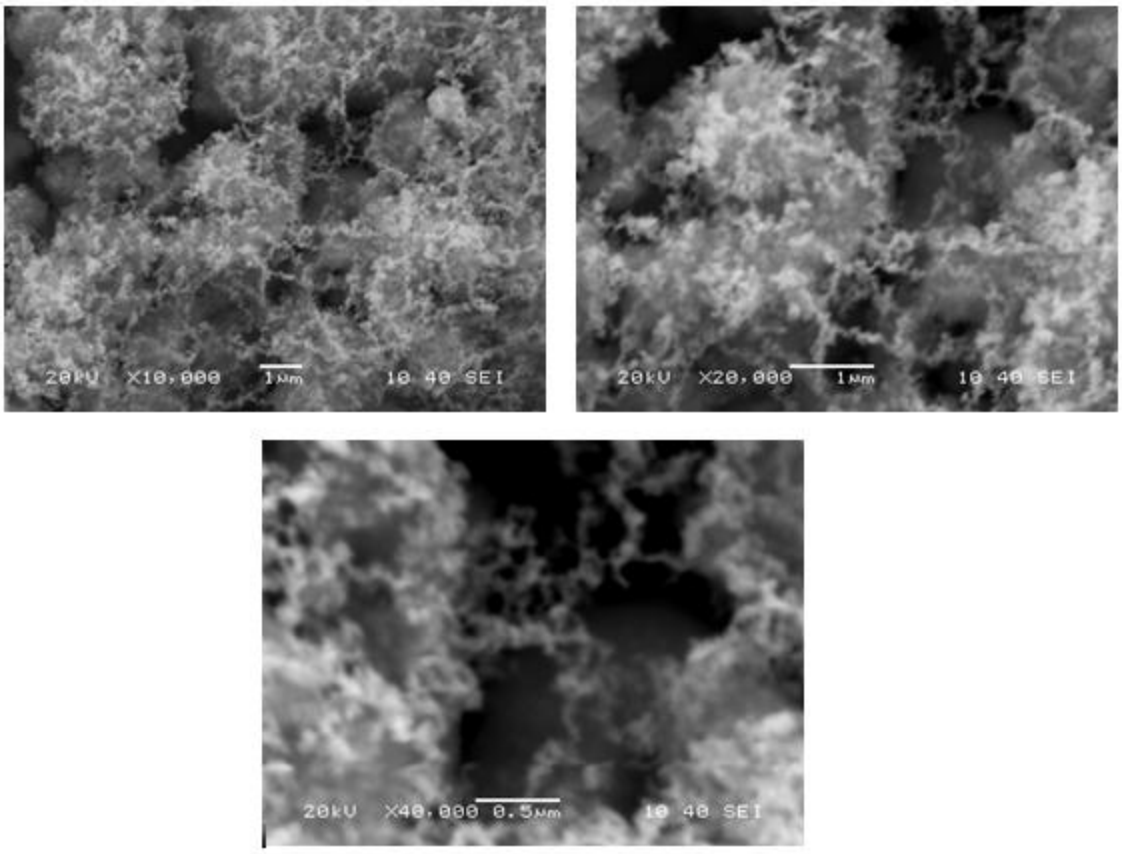


Figure A-5: Images showing the fine nanoparticle network generated

# Appendix B: Nanoparticle networks from NiO microparticles

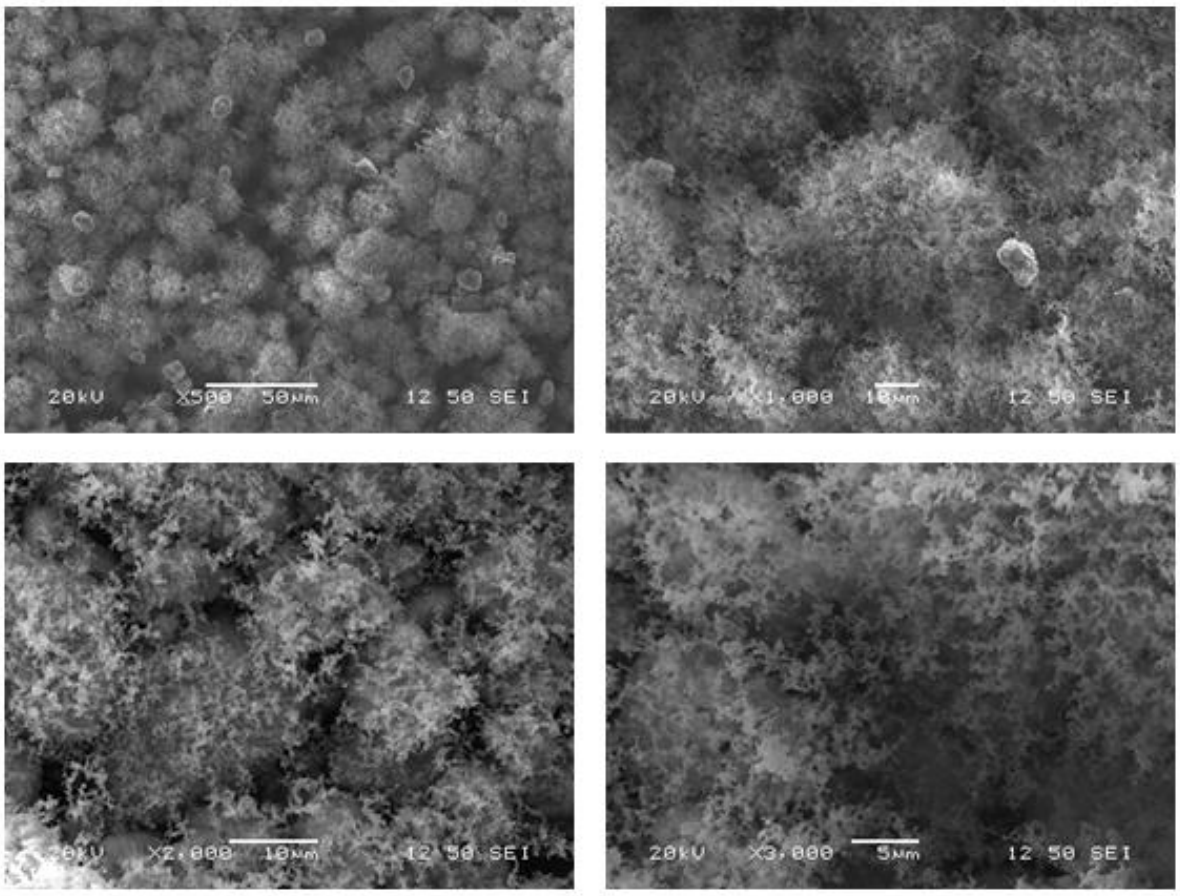


Figure B-1: Nanoparticle network generated by ablation of NiO microparticles

# Appendix C: Nanoparticle networks from ZnO microparticles

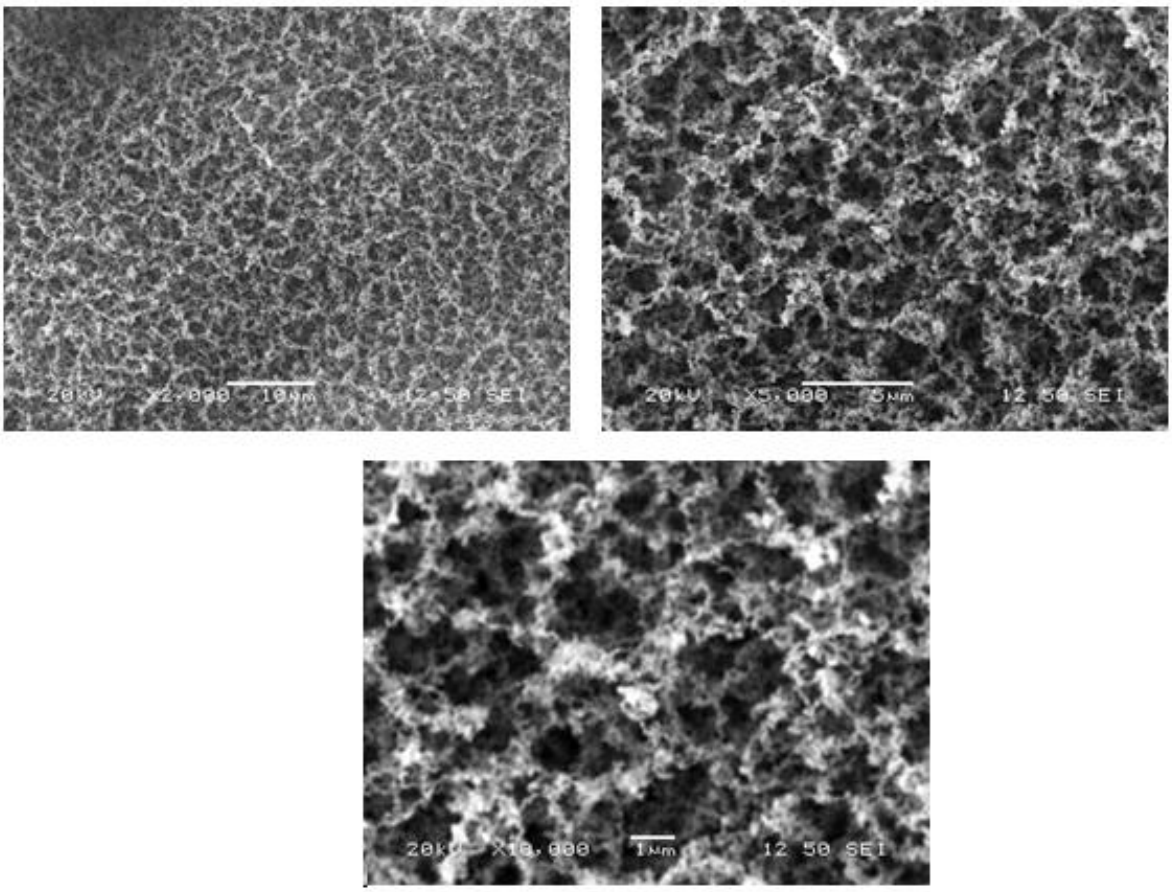


Figure C-1: Nanoparticle network generated by ablation of ZnO microparticles

# Appendix D: XRD analysis of Nickel Oxide (NiO) microparticles

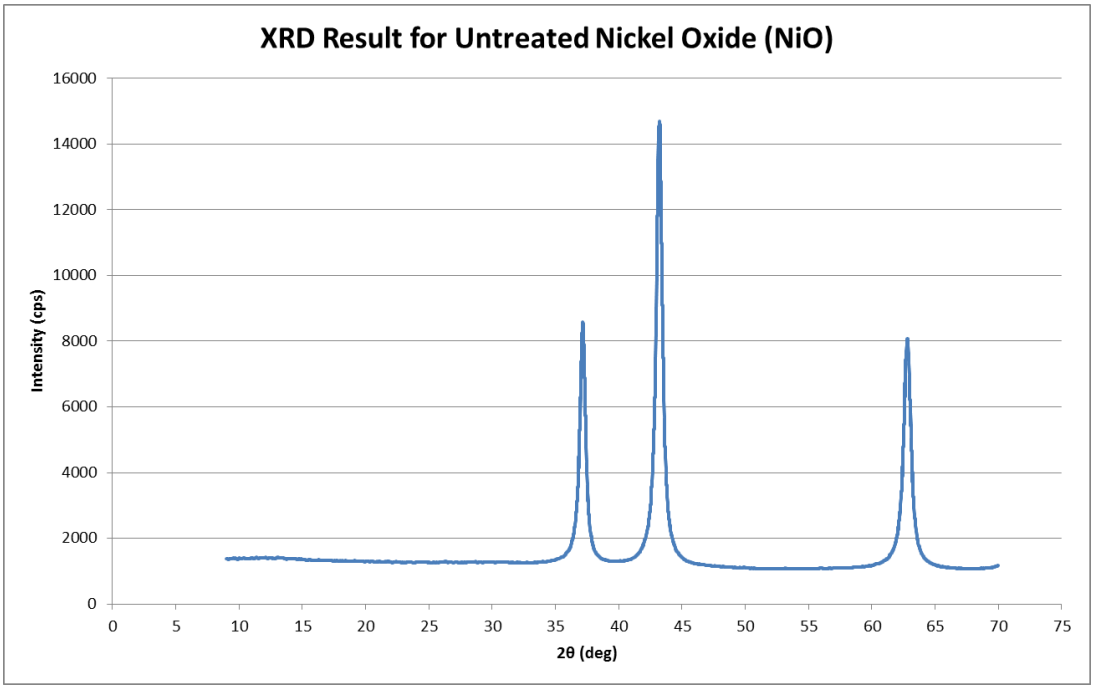


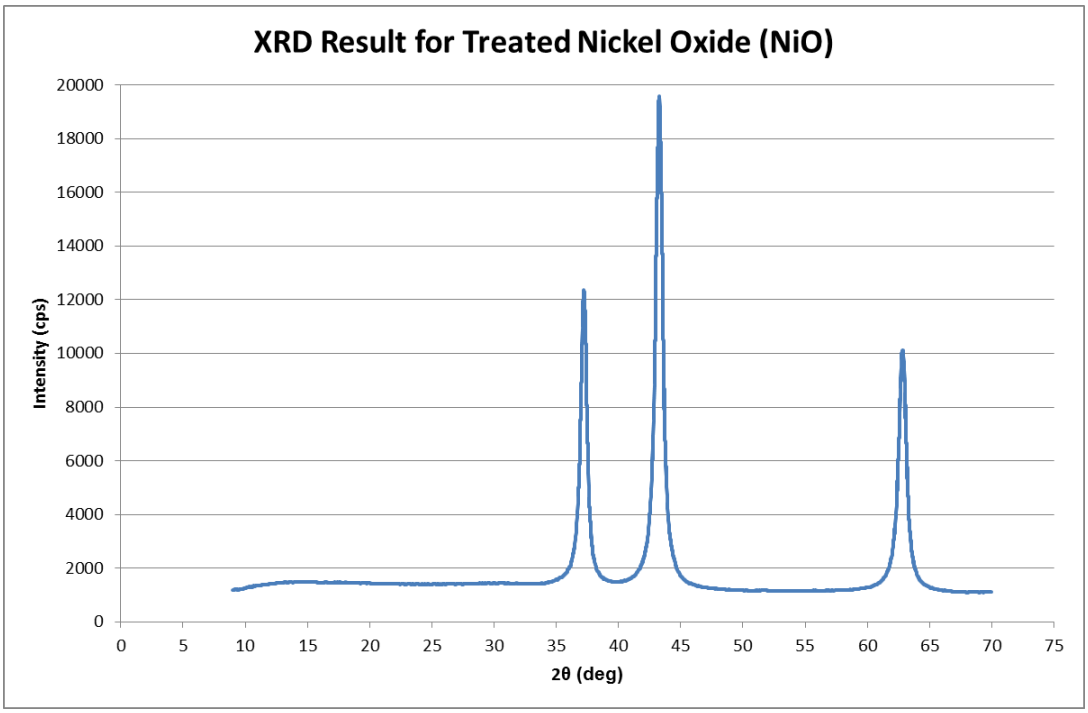

# Appendix E: JCPDS – International Centre for Diffraction Data Datasheet for $Pb_3O_4$

89-1947 Wavelength= 1.54184 C

Pb3O4

Lead Oxide

Minium, syn

Rad.: CuKa1 λ: 1.54060 Filter: d-sp: Calculated

Cut off: 17.7 Int.: Calculated I/Icor.: 13.17

Ref: Calculated from ICSD using POWD-12++

Ref: Gavarri, J.R., Weigel, D., C. R. Seances Acad. Sci., Ser. C, 275, 1267 (1972)

Sys.: Tetragonal S.G.: $P4_2/mbc$ (135)

a: 8.811(5) b: c: 6.563(5) A: C: 0.7449

α: β: γ: Z: 4 mp:

Ref: Ibid.

Dx: 8.938 Dm: 9.050

Peak height intensity. R-factor: 0.067. PSC: tP28. See PDF 71-561, 73-532 and 76-1799. Calc. density unusual but tolerable. At least one TF implausible. Mwt: 685.60. Volume[CD]: 509.51.

| 2θ | Int | h | k | l | 2θ | Int | h | k | l |
|---|---|---|---|---|---|---|---|---|---|
| 14.216 | 130 | 1 | 1 | 0 | 47.539 | 167 | 2 | 1 | 3 |
| 20.156 | 17 | 2 | 0 | 0 | 48.226 | 8 | 4 | 2 | 1 |
| 22.565 | 8 | 2 | 1 | 0 | 49.861 | 210 | 4 | 0 | 2 |
| 24.334 | 22 | 2 | 0 | 1 | 50.999 | 8 | 4 | 1 | 2 |
| 26.382 | 999* | 2 | 1 | 1 | 52.119 | 217 | 3 | 3 | 2 |
| 27.175 | 52 | 0 | 0 | 2 | 52.993 | 21 | 5 | 1 | 0 |
| 28.656 | 128 | 2 | 2 | 0 | 53.869 | 10 | 4 | 3 | 1 |
| 30.796 | 366 | 1 | 1 | 2 | 54.310 | 13 | 4 | 2 | 2 |
| 32.125 | 470 | 3 | 1 | 0 | 54.948 | 5 | 5 | 1 | 1 |
| 34.068 | 242 | 2 | 0 | 2 | 56.050 | 55 | 0 | 0 | 4 |
| 34.986 | 3 | 3 | 1 | 1 | 56.221 | 30 | 5 | 2 | 0 |
| 35.604 | 2 | 2 | 1 | 2 | 56.455 | 13 | 3 | 2 | 3 |
| 36.778 | 17 | 3 | 2 | 0 | 58.103 | 107 | 5 | 2 | 1 |
| 39.343 | 43 | 3 | 2 | 1 | 58.103 | | 1 | 1 | 4 |
| 39.903 | 51 | 2 | 2 | 2 | 59.333 | 43 | 4 | 4 | 0 |
| 40.972 | 16 | 4 | 0 | 0 | 59.546 | 24 | 4 | 3 | 2 |
| 42.293 | 1 | 4 | 1 | 0 | 59.546 | | 4 | 0 | 3 |
| 42.565 | 1 | 3 | 1 | 2 | 60.183 | 3 | 2 | 0 | 4 |
| 43.328 | 4 | 4 | 0 | 1 | 60.559 | 71 | 5 | 1 | 2 |
| 43.581 | 8 | 3 | 3 | 0 | 60.559 | | 4 | 1 | 3 |
| 44.592 | 88 | 4 | 1 | 1 | 61.352 | 15 | 5 | 3 | 0 |
| 46.070 | 96 | 4 | 2 | 0 | 63.138 | 9 | 5 | 3 | 1 |
| 46.324 | 21 | 3 | 2 | 2 | 63.333 | 48 | 6 | 0 | 0 |
| 46.324 | | 2 | 0 | 3 | 63.550 | 26 | 5 | 2 | 2 |
| 63.550 | | 4 | 2 | 3 | 85.160 | 3 | 7 | 3 | 1 |
| 64.152 | 18 | 2 | 2 | 4 | 85.519 | 5 | 7 | 2 | 2 |
| 64.310 | 12 | 6 | 1 | 0 | 86.071 | 21 | 4 | 4 | 4 |
| 65.089 | 3 | 6 | 0 | 1 | 86.408 | 12 | 4 | 0 | 5 |
| 66.086 | 98 | 6 | 1 | 1 | 86.408 | | 6 | 3 | 3 |
| 66.086 | | 3 | 1 | 4 | 87.145 | 8 | 4 | 1 | 5 |
| 67.197 | 3 | 6 | 2 | 0 | 87.828 | 14 | 6 | 5 | 1 |
| 68.145 | 1 | 5 | 4 | 0 | 87.828 | | 5 | 3 | 4 |
| 68.343 | 18 | 5 | 3 | 2 | 88.848 | 4 | 8 | 0 | 0 |
| 68.343 | | 4 | 3 | 3 | 89.584 | 27 | 6 | 0 | 4 |
| 68.935 | 4 | 6 | 2 | 1 | 89.584 | | 0 | 0 | 6 |
| 68.935 | | 3 | 2 | 4 | 89.909 | 16 | 7 | 3 | 2 |
| 69.295 | 3 | 5 | 1 | 3 | 89.909 | | 4 | 2 | 5 |
| 69.839 | 24 | 5 | 4 | 1 | | | | | |
| 70.219 | 2 | 6 | 0 | 2 | | | | | |
| 71.148 | 4 | 6 | 1 | 2 | | | | | |
| 71.730 | 5 | 4 | 0 | 4 | | | | | |
| 72.084 | 48 | 5 | 2 | 3 | | | | | |
| 72.652 | 1 | 4 | 1 | 4 | | | | | |
| 73.568 | 4 | 6 | 3 | 1 | | | | | |
| 73.568 | | 3 | 3 | 4 | | | | | |
| 73.908 | 27 | 6 | 2 | 2 | | | | | |
| 74.819 | 3 | 5 | 4 | 2 | | | | | |
| 75.389 | 32 | 4 | 2 | 4 | | | | | |
| 75.590 | 17 | 2 | 0 | 5 | | | | | |
| 76.494 | 33 | 5 | 5 | 0 | | | | | |
| 76.494 | 33 | 2 | 1 | 5 | | | | | |
| 76.640 | 18 | 5 | 3 | 3 | | | | | |
| 78.062 | 1 | 7 | 1 | 1 | | | | | |
| 78.238 | 1 | 6 | 4 | 0 | | | | | |
| 78.437 | 2 | 6 | 3 | 2 | | | | | |
| 78.437 | | 6 | 0 | 3 | | | | | |
| 79.134 | 5 | 7 | 2 | 0 | | | | | |
| 79.331 | 11 | 6 | 1 | 3 | | | | | |
| 79.849 | 5 | 6 | 4 | 1 | | | | | |
| 79.849 | | 4 | 3 | 4 | | | | | |
| 80.771 | 12 | 7 | 2 | 1 | | | | | |
| 80.771 | | 5 | 1 | 4 | | | | | |
| 80.968 | 6 | 3 | 1 | 5 | | | | | |
| 81.998 | 1 | 6 | 2 | 3 | | | | | |
| 82.872 | 53 | 7 | 1 | 2 | | | | | |
| 82.872 | 53 | 5 | 4 | 3 | | | | | |
| 83.571 | 33 | 7 | 3 | 0 | | | | | |
| 83.571 | | 3 | 2 | 5 | | | | | |
| 84.638 | 43 | 6 | 4 | 2 | | | | | |

# Appendix F: List of Publications

The following is the list of journal articles from the research conducted for this thesis work:

1. **P. S. Waraich**, B. Tan and K. Venkatakrishnan, "Laser ablation of microparticles for nanostructure generation," *Journal of Nanoparticle Research,* pp. 1-6, 2011

2. **P. S. Waraich**, B. Tan and K. Venkatakrishnan, "Al-NiO 3D nanostructure alloy by agglomeration of nanoparticles using mega-hertz frequency femtosecond laser," (To be submitted September 2011)

# References

[1] A. N. Goldstein, C. M. Echer and A. P. Alivisatos, "Melting in semiconductor nanocrystals," *Science,* vol. 256, pp. 1425-1427, 1992.

[2] S. H. Tolbert and A. P. Alivisatos, "High-pressure structural transformations in semiconductor nanocrystals," *Annu. Rev. Phys. Chem.,* vol. 46, pp. 595-625, 1995.

[3] K. Ishikawa, K. Yoshikawa and N. Okada, "Size effect on the ferroelectric phase transition in PbTiO3 ultrafine particles," *Physical Review B,* vol. 37, pp. 5852-5855, 1988.

[4] J. Horváth, R. Birringer and H. Gleiter, "Diffusion in nanocrystalline material," *Solid State Commun,* vol. 62, pp. 319-322, 1987.

[5] X. Y. Qin, B. M. Wu, Y. L. Du, L. D. Zhang and H. X. Tang, "An experimental study on thermal diffusivity of nanocrystalline Ag," *Nanostructured Materials,* vol. 7, pp. 383-391, 1996.

[6] H. W. Sarkas, S. T. Arnold, J. H. Hendricks, L. H. Kidder, C. A. Jones and K. H. Bowen, "An investigation of catalytic activity in mixed metal oxide nanophase materials," *Zeitschrift Für Physik D Atoms, Molecules and Clusters,* vol. 26, pp. 46-50, 1993.

[7] G. Hodes, A. Albu-Yaron, F. Decker and P. Motisuke, "Three-dimensional quantum-size effect in chemically deposited cadmium selenide films," *Physical Review B,* vol. 36, pp. 4215-4221, 1987.

[8] F. E. Kruis, H. Fissan and A. Peled, "Synthesis of nanoparticles in the gas phase for electronic, optical and magnetic applications--a review," *J. Aerosol Sci.,* vol. 29, pp. 511-535, 1998.

[9] M. De, P. S. Ghosh and V. M. Rotello, "Applications of nanoparticles in biology," *Adv Mater,* vol. 20, pp. 4225-4241, 2008.

[10] F. A. Volkening, M. N. Naidoo, G. A. Candela, R. L. Holtz and V. Provenzano, "Characterization of nanocrystalline palladium for solid state gas sensor applications," *Nanostructured Materials,* vol. 5, pp. 373-382, 1995.

[11] H. Ogawa, A. Abe, M. Nishikawa and S. Hayakawa, "ELECTRICAL PROPERTIES OF TIN OXIDE ULTRAFINE PARTICLE FILMS." *J. Electrochem. Soc.,* vol. 128, pp. 2020-2025, 1981.

[12] P. N. Njoki, "Metal and alloy nanoparticles: Synthesis, properties and applications," *ProQuest Dissertations and Theses,* 2007.

[13] S. Iwama, K. Hayakawa and T. Arizumi, "Ultrafine powders of TiN and AlN produced by a reactive gas evaporation technique with electron beam heating," *J. Cryst. Growth,* vol. 56, pp. 265-269, 1982.

[14] C. Kaito, K. Fujita and M. Shiojiri, "Growth of CdS smoke particles prepared by evaporation in inert gases," *J. Appl. Phys.,* vol. 47, pp. 5161-5166, 1976.

[15] M. S. El-Shall, "Laser vaporization for the synthesis of nanoparticles and polymers containing metal participates," *Appl. Surf. Sci.,* vol. 106, pp. 347-355, 1996.

[16] C. Lam, Y. F. Zhang, Y. H. Tang, C. S. Lee, I. Bello and S. T. Lee, "Large-scale synthesis of ultrafine Si nanoparticles by ball milling," *J. Cryst. Growth,* vol. 220, pp. 466-470, 12, 2000.

[17] T. G. Dietz, M. A. Duncan, D. E. Powers and R. E. Smalley, "Laser production of supersonic metal cluster beams," *J. Chem. Phys.,* vol. 74, pp. 6511-6512, 1981.

[18] M. Fumitaka, J. Kohno, Y. Takeda, T. Kondow and H. Sawabe, "Structure and Stability of Silver Nanoparticles in Aqueous Solution Produced by Laser Ablation," *The Journal of Physical Chemistry B,* vol. 104, pp. 8333-8337, 09/01, 2000.

[19] M. Fumitaka, J. Kohno, Y. Takeda, T. Kondow and H. Sawabe, "Formation of Gold Nanoparticles by Laser Ablation in Aqueous Solution of Surfactant," *The Journal of Physical Chemistry B,* vol. 105, pp. 5114-5120, 06/01, 2001.

[20] Y. Chen and C. Yeh, "Laser ablation method: Use of surfactants to form the dispersed Ag nanoparticles," *Colloids Surf. Physicochem. Eng. Aspects,* vol. 197, pp. 133-139, 2002.

[21] A. V. Kabashin and M. Meunier, "Synthesis of colloidal nanoparticles during femtosecond laser ablation of gold in water," *J. Appl. Phys.,* vol. 94, pp. 7941-7943, 2003.

[22] T. Tsuji, K. Iryo, N. Watanabe and M. Tsuji, "Preparation of silver nanoparticles by laser ablation in solution: influence of laser wavelength on particle size," *Appl. Surf. Sci.,* vol. 202, pp. 80-85, 12/15, 2002.

[23] S. Amoruso, R. Bruzzese, N. Spinelli, R. Velotta, M. Vitiello, X. Wang, G. Ausanio, V. Iannotti and L. Lanotte, "Generation of silicon nanoparticles via femtosecond laser ablation in vacuum," *Appl. Phys. Lett.,* vol. 84, pp. 4502-4504, 2004.

[24] S. Amoruso, G. Ausanio, R. Bruzzese, M. Vitiello and X. Wang, "Femtosecond laser pulse irradiation of solid targets as a general route to nanoparticle formation in a vacuum," *Physical Review B - Condensed Matter and Materials Physics,* vol. 71, pp. 1-4, 2005.

[25] C. Juang, H. Cai, M. F. Becker, J. W. Keto and J. R. Brock, "Synthesis of ultrafine glass particles by laser ablation of microspheres," *Nanostructured Materials,* vol. 4, pp. 569-575, 9, 1994.

[26] M. Becker, J. Brock, H. Cai, D. Henneke, J. Keto, J. Lee, W. Nichols and H. Glicksman, "Metal nanoparticles generated by laser ablation," *Nanostructured Materials,* vol. 10, pp. 853-863, 1998.

[27] H. Cai, N. Chaudhary, J. Lee, M. F. Becker, J. R. Brock and J. W. Keto, "Generation of metal nanoparticles by laser ablation of microspheres," *J. Aerosol Sci.,* vol. 29, pp. 627-636, 6/1, 1998.

[28] W. T. Nichols, G. Malyavanatham, D. E. Henneke, D. T. O'Brien, M. F. Becker and J. W. Keto, "Bimodal Nanoparticle Size Distributions Produced by Laser Ablation of Microparticles in Aerosols," *Journal of Nanoparticle Research,* vol. 4, pp. 423-432, 2002.

[29] X. Liu, D. Du and G. Mourou, "Laser ablation and micromachining with ultrashort laser pulses," *Quantum Electronics, IEEE Journal of,* vol. 33, pp. 1706-1716, 1997.

[30] N. Semaltianos, "Nanoparticles by Laser Ablation," *Critical Reviews in Solid State and Materials Sciences,* vol. 35, 2010.

[31] S. Manickam, K. Venkatakrishnan, B. Tan and V. Venkataramanan, "Study of silicon nanofibrous structure formed by femtosecond laser irradiation in air," *Optics Express,* vol. 17, pp. 13869-13874, 2009.

[32] B. Tan and K. Venkatakrishnan, "Synthesis of fibrous nanoparticle aggregates by femtosecond laser ablation in air," *Optics Express,* vol. 17, pp. 1064-1069, 2009.

[33] M. Sivakumar, K. Venkatakrishnan and B. Tan, "Synthesis of glass nanofibers using femtosecond laser radiation under ambient condition," *Nanoscale Research Letters,* vol. 4, pp. 1263-1266, 2009.

[34] S. Panchatsharam, B. Tan and K. Venkatakrishnan, "Femtosecond laser-induced shockwave formation on ablated silicon surface," *J. Appl. Phys.,* vol. 105, 2009.

[35] R. Sattari, C. Dieling, S. Barcikowski and B. Chichkov, "Laser-based fragmentation of microparticles for nanoparticle generation," *J.Laser Micro.Nanoengineer,* vol. 3, pp. 100–105, 2008.

[36] D. Jang, B. Oh and D. Kim, "Generation of metal nanoparticles by laser ablation of metal microparticles and plume dynamics," in *Proceedings of SPIE,* 2002, pp. 1024.

[37] J. Lee, M. F. Becker and J. W. Keto, "Dynamics of laser ablation of microparticles prior to nanoparticle generation," *J. Appl. Phys.,* vol. 89, pp. 8146-8152, 2001.

[38] R. Ganeev, L. Elouga Bom and T. Ozaki, "Deposition of nanoparticles during laser ablation of nanoparticle-containing targets," *Appl. Phy. B,* vol. 96, pp. 491-498, 2009.

[39] B. Y. Tsaur and J. W. Mayer, "Supersaturated metastable Ag-Ni solid solutions formed by ion beam mixing," *Appl. Phys. Lett.*, vol. 37, pp. 389-392, 1980.

[40] S. H. Liou, S. Malhotra, Z. S. Shan, D. J. Sellmyer, S. Nafis, J. A. Woollam, C. P. Reed, R. J. Deangelis and G. M. Chow, "The process-controlled magnetic properties of nanostructured Co/Ag composite films," *J. Appl. Phys.*, vol. 70, pp. 5882-5884, 1991.

[41] M. P. Andrews and S. C. O'Brien, "Gas-phase "molecular alloys" of bulk immiscible elements: FexAgy," *J. Phys. Chem.*, vol. 96, pp. 8233-8241, 1992.

[42] S. D. Dahlgren, J. W. Patten and M. T. Thomas, "The metallurgical characterization of coatings," *Thin Solid Films*, vol. 53, pp. 41-54, 1978.

[43] H. Gleiter, "Nanocrystalline materials," *Progress in Materials Science*, vol. 33, pp. 223-315, 1989.

[44] J. J. Burton, E. Hyman and D. G. Fedak, "Surface segregation in alloys," *Journal of Catalysis*, vol. 37, pp. 106-113, 1975.

[45] D. W. Hoffman, "Phase stability of alloy catalyst particles," *Journal of Catalysis*, vol. 27, pp. 374-378, 1972.

[46] D. Poondi and J. Singh, "Synthesis of metastable silver-nickel alloys by a novel laser-liquid-solid interaction technique," *J. Mater. Sci.*, vol. 35, pp. 2467-2476, 2000.

[47] A. T. Izgaliev, A. V. Simakin and G. A. Shafeev, "Formation of the alloy of Au and Ag nanoparticles upon laser irradiation of the mixture of their colloidal solutions," *Quantum Electronics*, vol. 34, pp. 47-50, 2004.

[48] Y. Chen, Y. Tseng and C. Yeh, "Laser-induced alloying Au-Pd and Ag-Pd colloidal mixtures: the formation of dispersed Au/Pd and Ag/Pd nanoparticles," *J. Mater. Chem.*, vol. 12, pp. 1419-1422, 2002.

[49] J. Zhang, J. Worley, S. Dénommée, C. Kingston, Z. J. Jakubek, Y. Deslandes, M. Post, B. Simard, N. Braidy and G. A. Botton, "Synthesis of Metal Alloy Nanoparticles in Solution by Laser Irradiation of a Metal Powder Suspension," *The Journal of Physical Chemistry B,* vol. 107, pp. 6920-6923, 07/01, 2003.

[50] J. H. Hodak, A. Henglein, M. Giersig and G. V. Hartland, "Laser-Induced Inter-Diffusion in AuAg Coreâ^'Shell Nanoparticles," *The Journal of Physical Chemistry B,* vol. 104, pp. 11708-11718, 12/01, 2000.

[51] I. Gallardo, K. Hoffmann and J. Keto, "CdSe & ZnS core/shell nanoparticles generated by laser ablation of microparticles," *Appl. Phys. A,* vol. 94, pp. 65-72, 2009.

[52] P. S. Waraich, B. Tan and K. Venkatakrishnan, "Laser ablation of microparticles for nanostructure generation," *Journal of Nanoparticle Research,* pp. 1-6, 2011.

[53] M. Shirk and P. Molian, "A review of ultrashort pulsed laser ablation of materials," *J. Laser Appl.,* vol. 10, pp. 18, 1998.

[54] M. Alubaidy, K. Venkatakrishnan and B. Tan, "On the formation of titanium/titanium oxide nanofibrous structures and nanospheres using femtosecond laser in air," *Nano,* vol. 6, pp. 123-130, 2011.